Nitrate-driven dark oxygen production by diverse deep-sea microorganisms

Rikuan Zheng[1,2,3#], Chong Wang[1,2,3#], Hongliang Wang[4], Haibin Qi[4], Chaomin Sun[1,2,3,5*]

[1]CAS and Shandong Province Key Laboratory of Experimental Marine Biology & Center of Deep Sea Research, Institute of Oceanology, Chinese Academy of Sciences, Qingdao, China

[2]Laboratory for Marine Biology and Biotechnology, Qingdao National Laboratory for Marine Science and Technology Center, Qingdao, China

[3]Center of Ocean Mega-Science, Chinese Academy of Sciences, Qingdao, China

[4]National Deep Sea Center, Qingdao, China

[5]College of Earth Science, University of Chinese Academy of Sciences, Beijing, China

[#] These authors contributed equally to this work

[*] Corresponding author

Chaomin Sun Tel.: +86 532 82898857; fax: +86 532 82898857.

E-mail address: sunchaomin@qdio.ac.cn

Key words: Dark oxygen production, deep sea, dissimilatory nitrate reduction, denitrification, Great Oxidation Event

Abstract

To date, only three biotic pathways for light-independent oxygen (i.e. dark oxygen) production: chlorate dismutation, nitric oxide dismutation, and methanobactin-dependent lysis of water. Oxygen has been shown to be produced and consumed in dark and apparently anoxic environments, as evidenced by its prevalence in deep-sea surface sediments. However, the microbial communities and pathways driving deep-sea dark oxygen production (DOP) remain unclear. Here we identified a novel DOP pathway driven by the process of dissimilatory nitrate reduction to ammonium (DNRA) in two deep-sea *Deferribacterota* strains. DOP of *Deferribacterota* strains potentially promotes the formation of manganese nodules, as well as affects the growth and metabolism of both deep-sea aerobic and anaerobic microbes, indicating the considerable impacts of microbial DOP in shaping deep-sea geological and ecological systems. We also cultured several deep-sea DOP members belonging to *Campylobacterota*, *Deinococcota*, and *Pseudomonadota* phyla, which generate dark oxygen through unidentified nitrate-driven pathways. Coupled with previous geological evidences, our results indicate that nitrate-driven dark oxygen, alongside photosynthetic oxygen, conjointly contributed to early Earth's oxygenation, driving the Great Oxidation Event (GOE). Overall, our findings offer novel evidence regarding deep-sea oxygen source, provide new insights into the origins of early Earth's oxygen, and expand our perspective for terraforming planets.

Photosynthetic oxygen is considered to be the primary source of oxygen on Earth (*1, 2*). Light-independent abiotic or biotic process also contributes to oxygen production, particularly during early Earth history (oxygen-free age), a process termed dark oxygen production (DOP) (*3*). Recent studies have suggested that dark oxygen-generating microorganisms may play a significant role in certain anoxic environments (*4*). Microbial DOP has not been extensively studied, with only three known pathways: chlorite (ClO_2^-) dismutation ($ClO_2^- \rightarrow Cl^- + O_2$) (*5*), nitric oxide (NO) dismutation ($2NO_2^- \rightarrow 2NO \rightarrow N_2 + O_2$ or $4NO_2^- \rightarrow 4NO \rightarrow 2N_2O + O_2$) (*6, 7*), and water lysis by methanobactins (*8*). In addition, reactive oxygen species (e.g. H_2O_2) can be disproportionated to O_2 and H_2O both biotically, via enzymes such as superoxide dismutase and catalase, and abiotically, by ferrous iron and other reduced metals (*9, 10*). However, due to low levels of reactive oxygen species *in vivo*, the resulting oxygen production is negligible and difficult to detect, rendering it insignificant compared to the other three biotic DOP pathways, particularly in most low-temperature, anoxic systems (*3*).

Growing geochemical and microbiological evidences suggest that DOP is a significant and widespread, yet overlooked, process in nominally anoxic environments, including groundwater, subsurface, lake, wetland, and marine ecosystems. Groundwater and subsurface environments harbor strictly aerobic methanotrophs (*11*), methanotrophic *Methylobacter* (*4*), and other viable aerobic heterotrophs (*4*), indicative of relatively oxidizing conditions (*12*). Aerobic methanotrophs have also been detected in anoxic sediments of Lake Constance, Germany (*13*) and at a methane seep in Lake Qalluuraq, Alaska (*14*) (sediments up to 70 cm depth). Likewise, aerobically methanotrophic community has been observed in an Arctic wetland, exhibiting peak activity in the anoxic and transition zones (*15*). Aerobic activity has also been detected several meters below the seafloor within the permanently anoxic Arabian Sea oxygen minimum zone (OMZ), where *Nitrosopumilus* archaeon (*7*) (potential dark oxygen producer), *nod* genes (*6*) (encoding nitric oxide dismutase for DOP), and transcribed oxidase genes were also found (*16*). Moreover, in deep-sea methane seeps and mud volcanoes, aerobic methanotrophs are abundant in methane-rich sediments well below

the measurable oxygen penetration depth (*17, 18*). Not only microorganisms, animals (e.g. blind shrimp and *Alvinocaris* shrimp around deep-sea hydrothermal vents; squat lobsters and mussels around cold seeps) also widely distribute in the deep sea, suggesting substantial oxygen availability in these regions. What fascinates people is how does deep-sea oxygen derive from? Recent findings suggest that polymetallic nodules at the abyssal seafloor may produce dark oxygen through seawater electrolysis, although the mechanistic details remain unknown (*19*). This observation highlights the potential importance of DOP in deep-sea ecosystems and its implications for generating oxygenated habitats on other ocean worlds. Given that oxygen is prevalent in deep-sea surface sediments (*19*), we are curious to know whether and how does microbial DOP contribute to the deep-sea oxygen source?

Deep-sea *Deferribacterota* bacteria produce dark oxygen

To enrich deep-sea microorganisms possessing the capability of producing dark oxygen, we specially used a nitrate-containing medium because denitrification potentially drives microbial DOP (*6, 7, 20*) and nitrate is closely correlated to the content of deep-sea oxygen (*21*). The enrichment was incubated in anaerobic condition, and the oxygen indicator resazurin, whose reduced form dihydroresazurin transits from colorless to pink when it is oxidated to resorufin (fig. S1A), was supplemented in the medium to detect the presence of trace oxygen. Surprisingly, we indeed observed two anaerobic tubes supplemented with hydrothermal vents samples exhibited visible microbial growth and converted from colorless to pink (fig. S1B), suggesting these two enrichments might produce oxygen. Two rod-shaped bacterial strains (DY0037 and DY0609) were respectively purified from above two enrichments (fig. S1C) and identified as *Deferribacterota* phylum members (fig. S1D). To further confirm the oxygen production by *Deferribacterota* strains DY0037 and DY0609, we conducted scaled-up incubations in larger vessels. We observed the formation of gas bubbles in the anaerobic bottles over time (fig. S2A), accompanied by a gradual shift in medium color from colorless to pink (24 hours), and ultimately to deep red (48 hours) (Fig. 1A). This phenomenon was further corroborated by measurements of dissolved oxygen

using a liquid phase oxygen electrode. These analyses revealed a gradual increase in dissolved oxygen concentrations with culture growth, reaching approximately 70 μM (Fig. 1, B and C). Subsequently, strain DY0037 exhibited a decline in oxygen levels, indicating consumption, while strain DY0609 maintained a stable dissolved oxygen concentration likely due to its low oxygen-utilization capacity. The dissolved oxygen concentration is over 300-fold higher than that produced by a previously reported ammonia-oxidizing archaea via NO dismutation (*7*), and nearly exceeding the maximum dissolved oxygen level achievable in anoxic aquatic habitats (<60 μM) (*22*), as well as the upper limit of typical marine hypoxic conditions (2 mg/L or 63 μM) (*23*).

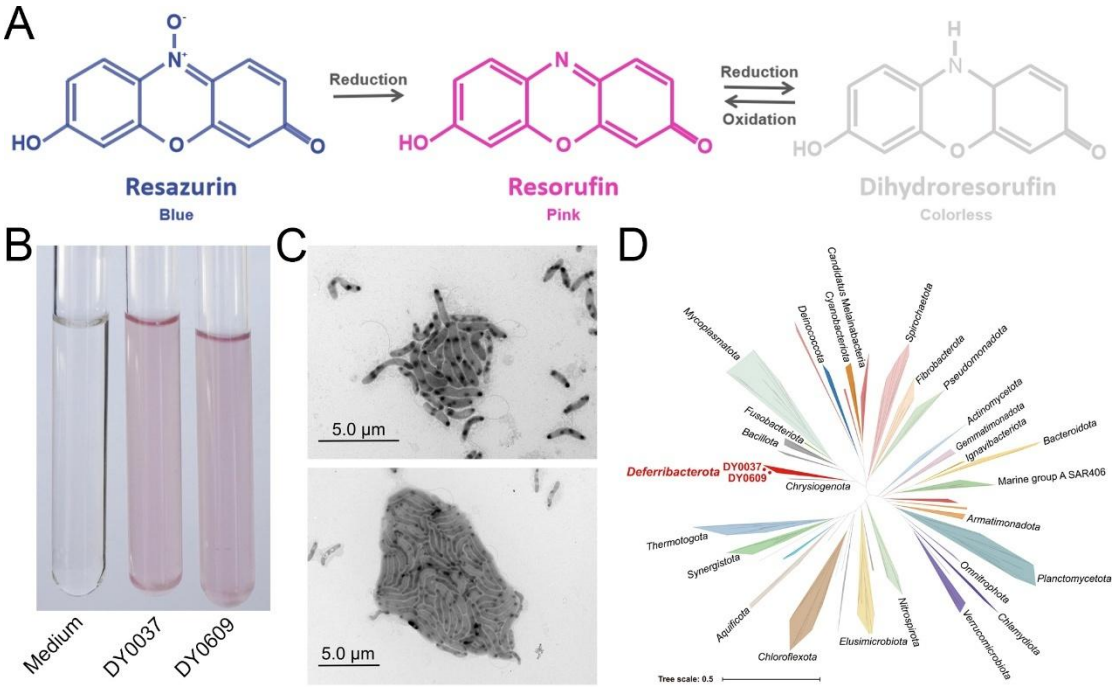

fig. S1. Isolation, morphology and phylogenetic affiliation of two deep-sea anaerobic bacteria possessing potential oxygen-production capability. (**A**) The oxygen indicator resazurin exhibits distinct color states depending on oxygen availability: blue (oxidized form, resazurin), pink (intermediate reduced form, resorufin), and colorless (fully reduced form, dihydroresorufin). (**B**) Observation of the color in the control medium and the same medium inoculated with deep-sea bacterial strain DY0037 or DY0609. (**C**) Transmission electron micrographs showing the morphology of strains DY0037 and DY0609. Bar is 5 μm. (**D**) Phylogenetic analysis of strains DY0037 and DY0609 based on full-length 16S rRNA gene sequences from some *Deferribacterota* members and other representative phyla. Scale bar, 0.5 substitutions per nucleotide position.

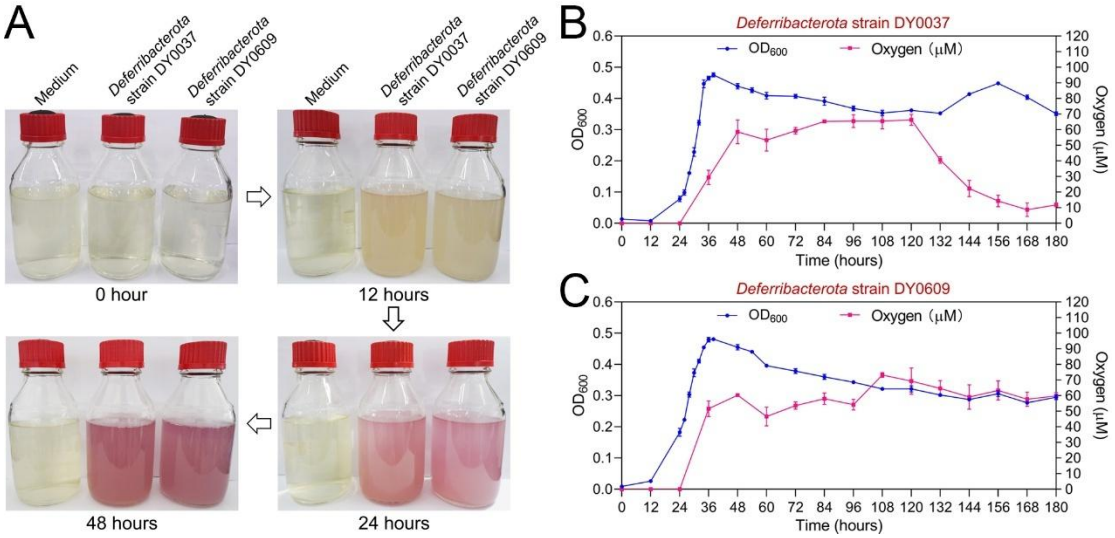

Fig. 1. Deep-sea *Deferribacterota* strains DY0037 and DY0609 produce oxygen during anaerobic growth. (**A**) Time-lapse images showing the culture medium transitioning from colorless (0 hour) to slightly pink (12 hours), pink (24 hours) and finally red (48 hours) during anaerobic growth of strains DY0037 and DY0609. (**B** and **C**) Growth curves and dissolved oxygen production profiles of strains DY0037 (B) and DY0609 (C).

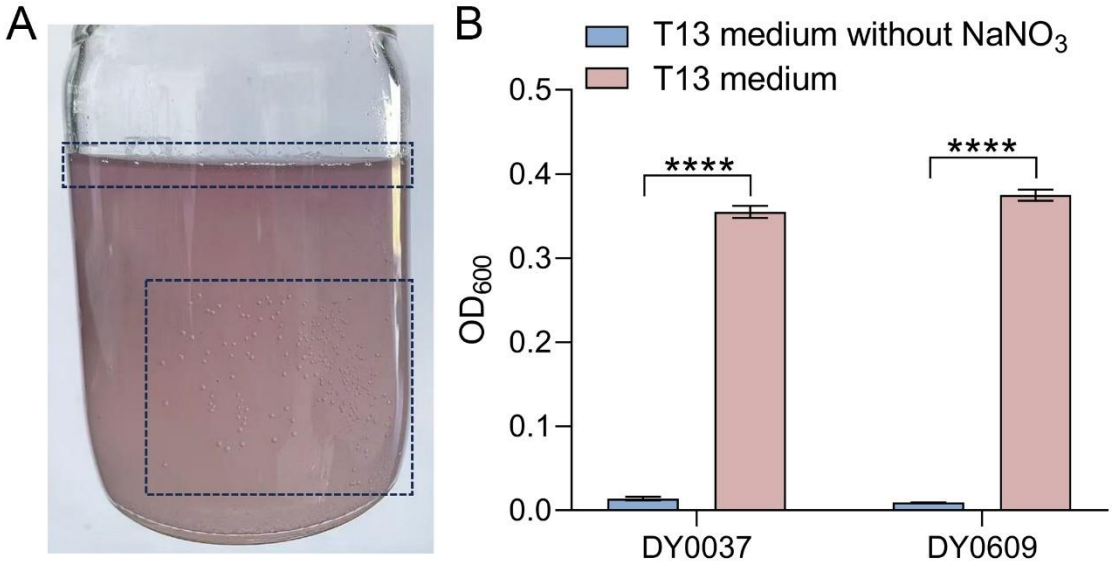

fig. S2. *Deferribacterota* strains DY0037 and DY0609 produce oxygen strictly dependent on the presence of nitrate. (**A**) Oxygen production is apparent on the inner walls and in the upper layer of the culture bottles (dashed boxes) during anaerobic cultivation of strains DY0037 and DY0609 in the nitrate-containing medium. (**B**) Growth profiles of strains DY0037 and DY0609 in T13 medium supplemented with and without sodium nitrate. Error bars show mean ± SD. ****$P < 0.0001$.

It is noting that the growth and oxygen production of two *Deferribacterota* strains are strictly dependent on nitrate (fig. S2B). In comparison, no growth or oxygen production was detected when cells were killed by high-temperature, high-pressure sterilization (fig. S3), ruling out the possibility of both abiotic oxygen production and oxygen intrusion into the incubation vessels. Furthermore, incubations of strains DY0037 and DY0609 in above nitrate-containing medium, with or without pyruvate supplementation, showed no significant difference in growth (fig. S4A) and dissolved oxygen production (fig. S4B). This result excluded oxygen production via H_2O_2 dismutation ($H_2O_2 \rightarrow H_2 + O_2$), as pyruvate abiotically scavenges H_2O_2 through decarboxylation (*24*). The absence of chlorate and chlorite in the culture medium and throughout the cultivation process also excluded the possibility of chlorite-dependent oxygen production. In addition, incubation of *Deferribacterota* strains in nitrate-containing medium revealed no significant difference in growth (fig. S4C) or dissolved oxygen production (fig. S4D) under dark and light conditions, indicating these two *Deferribacterota* strains produce dark oxygen. *Deferribacterota* bacteria are prevalent in deep-sea habitats (*25-27*), and are able to oxidize complex organic compounds and organic acids (mainly acetate) using a variety of electron acceptors (mainly nitrate) (*28*). Therefore, nitrate-dependent oxygen production may be widespread among *Deferribacterota* species, potentially contributing to oxygen availability across diverse deep-sea ecosystems.

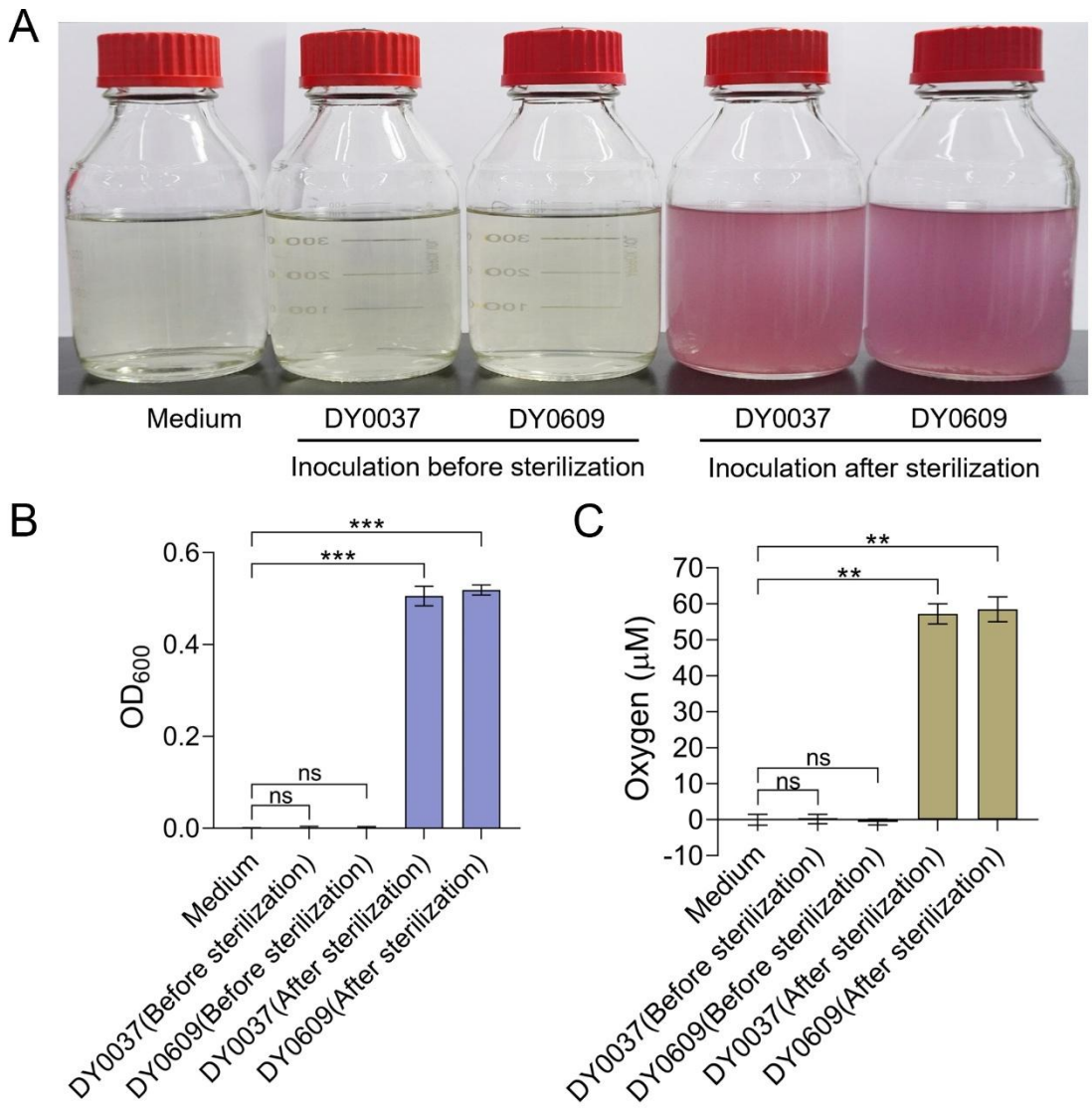

fig. S3. Ruling out the possibility of both abiotic oxygen production and oxygen intrusion into the incubation vessels during cultivation of *Deferribacterota* strains DY0037 and DY0609. (**A**) Photographs of culture medium after adding seed cultures of strains DY0037 and DY0609, both before and after sterilization, with uninoculated medium serving as the control. (**B**) Growth profiles of strains DY0037 and DY0609 following the addition of seed cultures before and after medium sterilization, compared to the control. (**C**) Dissolved oxygen levels measured following the addition of seed cultures of strains DY0037 and DY0609 before and after medium sterilization, with uninoculated medium serving as the control. Error bars show mean ± SD. $^{**}P < 0.01$, $^{***}P < 0.001$.

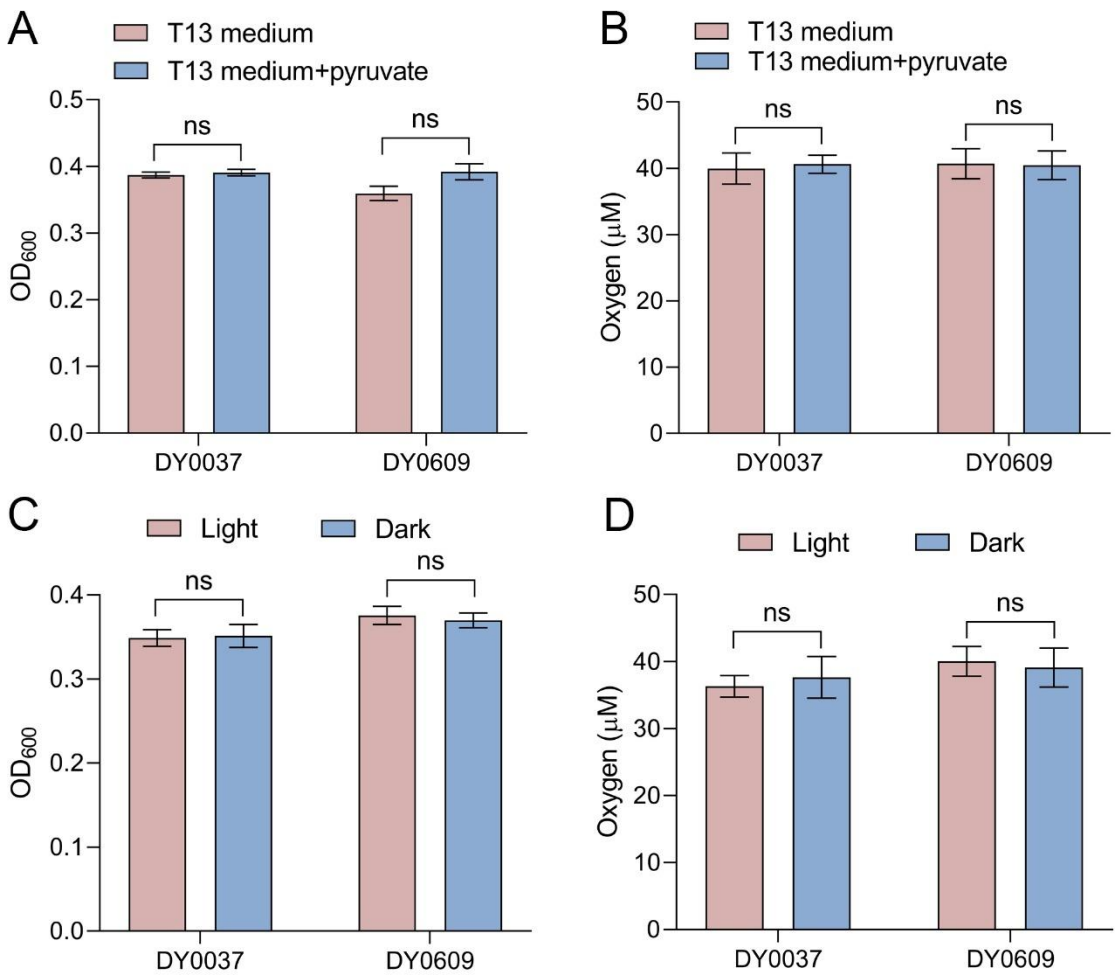

fig. S4. Ruling out the possibility of oxygen production via H_2O_2 dismutation in *Deferribacterota* strains DY0037 and DY0609. (**A**) Growth profiles of strains DY0037 and DY0609 in T13 medium with or without 0.2 mM pyruvate supplementation. (**B**) Dissolved oxygen concentrations of strains DY0037 and DY0609 in T13 medium with or without 0.2 mM pyruvate supplementation. (**C**) Growth profiles of strains DY0037 and DY0609 cultivated under light and dark conditions. (**D**) Dissolved oxygen concentrations of strains DY0037 and DY0609 cultivated under light and dark conditions. Error bars show mean ± SD. "ns" denotes no significant difference ($P > 0.05$).

Deferribacterota strains produce dark oxygen via a novel pathway

To elucidate the DOP pathway in *Deferribacterota* strains DY0037 and DY0609, we first sequenced their genomes and analyzed their nitrate reduction pathways, given that nitrate is necessary for growth and oxygen production of these two strains. Intriguingly, we found they both possess incomplete dissimilatory nitrate reduction to ammonia

185 (DNRA) and denitrification pathways, encoding only nitrate reductases (NapADGH
186 and NarGHIJK) and nitrous oxide reductase (NosZ) (Fig. 2A). Cultures grown with
187 ^{18}O-nitrate exhibited significantly elevated $^{18}O_2/^{16}O_2$ ratios compared to control
188 cultures (7.4-fold and 12.9-fold increases for strains DY0037 and DY0609,
189 respectively), confirming that both strains utilize nitrate for oxygen generation (Fig.
190 2B). Furthermore, the formation of abundant magnesium ammonium phosphate
191 mineral particles ($MgNH_4PO_4 \cdot 6H_2O$) was observed during cultivation, indicative of
192 substantial ammonium production (fig. S5). This observation, coupled with the
193 detection of ^{15}N-nitrate, ^{15}N-nitrite, and ^{15}N-ammonium accumulation (approximately
194 1.2, 2.1, and 1.5 mM for strain DY0037 and 1.1, 2.0, and 2.0 mM for strain DY0609,
195 respectively) in cultures amended with ^{15}N-nitrate (Fig. 2C), alongside the consumption
196 of ammonium during $MgNH_4PO_4 \cdot 6H_2O$ precipitation, strongly suggesting that both
197 strains perform DNRA process though the gene encoding enzyme catalyzing NO_2^- to
198 NH_4^+ has not been found in their genomes. Real-time monitoring of inorganic nitrogen
199 concentrations during culture growth revealed a marked increase in both ammonium
200 and dissolved oxygen concentrations concomitant with a decrease in nitrate
201 concentrations, while the total inorganic nitrogen content remained balanced (Fig. 2, D
202 and E), suggesting there is no generation of nitrogen-containing gas. Consistent with
203 these findings, transcriptomic analyses under high concentration of nitrate stress
204 demonstrated significant upregulation of genes encoding key enzymes related to nitrate
205 reduction (fig. S6). Taken together, these results indicate that strains DY0037 and
206 DY0609 can perform DNRA process under anaerobic condition, resulting in oxygen
207 production. Consequently, a novel DNRA-dependent oxygen production pathway in
208 *Deferribacterota* strains DY0037 and DY0609 is shown in Figure 2F, which is
209 thermodynamically feasible, distinct from previously reported NO dismutation during
210 denitrification (*6, 7*). In this pathway, following the reduction of nitrate to nitrite by the
211 nitrate reductase, an unidentified enzyme converts one molecule of nitrite to one
212 molecule of oxygen and one molecule of ammonium with the involvement of two
213 electrons (may partly derive from intra- or extracellular organic matter such as sodium
214 acetate) and four protons (may partly derive from water). Here we present evidence for

a fourth biotic pathway for DOP, potentially of considerable biological and geochemical significance. Considering *Deferribacterota* strains DY0037 and DY0609 lack canonical nitrite reductases, suggesting a novel enzyme mediating nitrite reduction to ammonium and O_2; however, the responsible gene remains unidentified. Future efforts will focus on developing a genetic system in anaerobic *Deferribacterota* bacteria to identify key genes controlling dark oxygen generation.

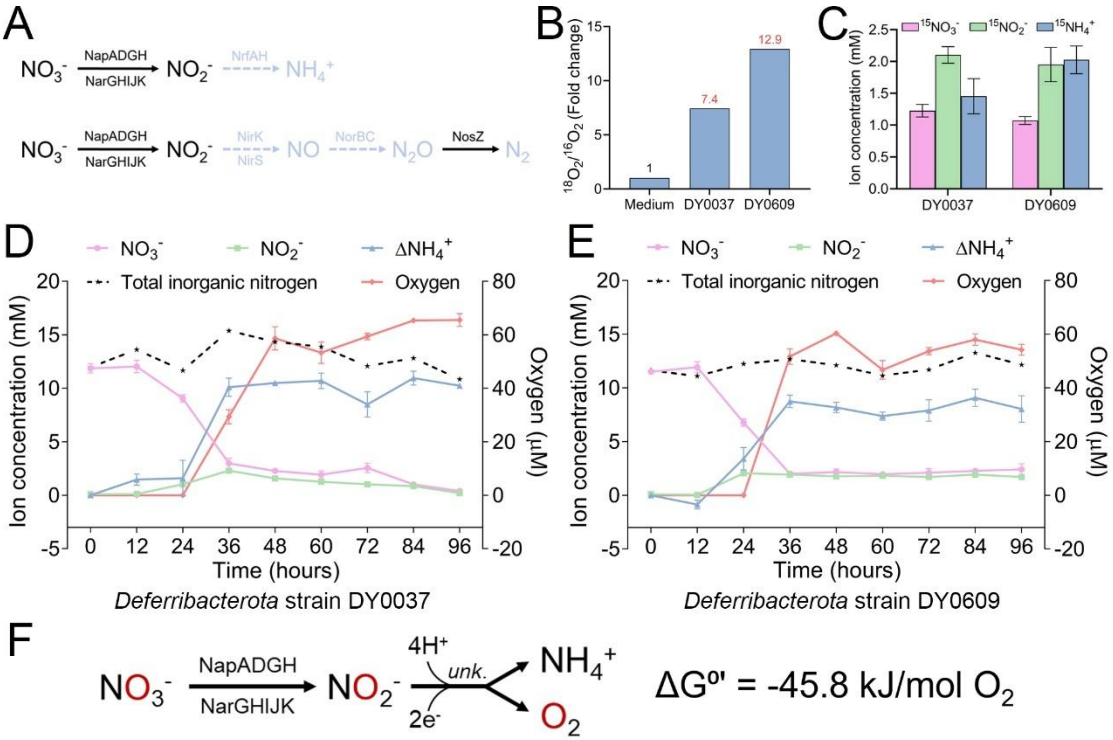

Fig. 2. *Deferribacterota* strains DY0037 and DY0609 produce dark oxygen through the DNRA-dependent pathway. (**A**) Genomic analysis of the DNRA and denitrification pathways in *Deferribacterota* strains DY0037 and DY0609. Solid black lines indicate the presence of relevant genes and intermediates, while dashed light blue lines denote the absence of relevant genes and intermediates. (**B**) Ratio of ^{18}O-labeled oxygen to ^{16}O-labeled oxygen measured in cultures supplemented with ^{18}O-labeled nitrate, with uninoculated medium as the control. (**C**) Concentrations of ^{15}N-labeled nitrate, nitrite, and ammonium during incubation of strains DY0037 and DY0609 in the medium supplemented with ^{15}N-labeled nitrate, with uninoculated medium serving as the control. (**D** and **E**) Concentrations of each inorganic nitrogen ion (NO_3^-, NO_2^-, NH_4^+), total inorganic nitrogen, and dissolved oxygen during cultivation of strains DY0037 (D) and DY0609 (E). ΔNH_4^+ indicates the difference between the final and initial concentrations of NH_4^+

present in the culture. (**F**) The proposed DNRA-dependent pathway for dark oxygen production in strains DY0037 and DY0609: nitrate is reduced to nitrite by the nitrate reductase (NarGHIJK or NapADGH). An unknown enzymatic process mediates the conversion of nitrite to oxygen and ammonium. This pathway requires two external electrons and four protons per produced O_2. Gibbs free energy (ΔG) refers to the O_2 generating step.

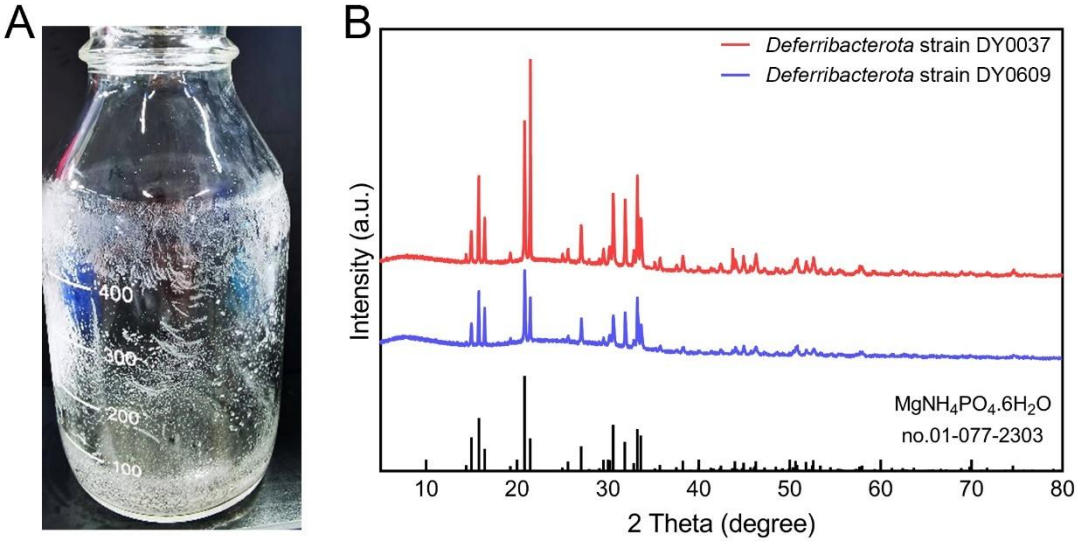

fig. S5. Characterization of minerals formed by *Deferribacterota* strains DY0037 and DY0609 during the course of oxygen production in the nitrate-containing medium. (**A**) Visual observation of abundant mineral formation during cultivation of strains DY0037 and DY0609. (**B**) X-ray diffraction (XRD) analysis of the minerals formed by strains DY0037 and DY0609.

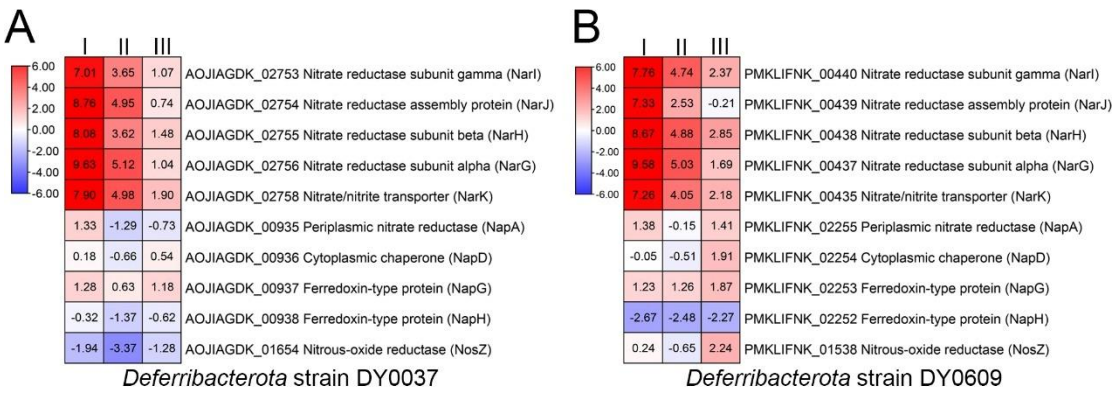

fig. S6. Transcriptomic analysis of the expression of nitrogen metabolism associated genes in *Deferribacterota* strains DY0037 and DY0609 in the medium containing varying concentrations of nitrate. Transcriptomic profiles of nitrogen metabolism associated genes in strains DY0037 (**A**) and DY0609 (**B**) under varying nitrate concentrations (0.1, 0.5, 1.0, and 3.0 g/L). "I" indicates the ratio of genes expression in strain DY0037 or DY0609 grown in the medium containing 0.5 g/L nitrate versus 0.1 g/L nitrate; "II" indicates the ratio of genes expression in strain DY0037 or DY0609 grown in the medium containing strain DY0037 or DY0609 grown in 1.0 g/L nitrate versus 0.1 g/L nitrate; "III" indicates the ratio of genes expression in strain DY0037 or DY0609 grown in the medium containing 3.0 g/L nitrate versus 0.1 g/L nitrate. The numbers in panels a and b represent the fold change of gene expression (by using the $\log_2$ value).

Geological and ecological impacts of deep-sea microbial dark oxygen

Nodule provinces, abundant with ferromanganese nodules, are well-known deep-sea geological features (*29*). Given that oxygen is important for manganese nodules formation (*30*), we thus ask whether oxygen produced by *Deferribacterota* strains could promote the formation of manganese nodules. Indeed, FESEM and TEM imaging showed that *Deferribacterota* strains DY0037 and DY0609 facilitated the formation of mineral precipitates in the presence of 20 mM Mn(II) (Fig. 3A and fig. S7, A and B.). EDS results showed the contents of both oxygen and manganese elements were the top two in the precipitates formed by strains DY0037 (Fig. 3B) and DY0609 (fig. S7C). XPS analysis revealed Mn(II):Mn(IV) ratios of 46.6%:53.4% and 48.4%:51.6% in the surface of minerals formed by strains DY0037 (Fig. 3C) and DY0609 (fig. S7D), respectively, suggesting that oxygen produced by two strains drive the oxidation of

Mn(II) to Mn(IV). EDS and XPS results were consistent in demonstrating the existence of MnO_2 in the minerals because Mn(IV) mainly exists in the formation of MnO_2. Given that MnO_2 is the major component of polymetallic nodules, we thus infer a potential role of oxygen-producing microorganisms in the formation of polymetallic nodules. Combining recent report of oxygen production within deep-sea polymetallic nodules (*19*) and our present findings, we hypothesize that oxygen-producing microorganisms may reside in these structures and contribute to the formation of polymetallic nodules and production of dark oxygen.

Considering strains DY0037 and DY0609 release free oxygen to the external environment, we next examined the effect of their DOP on other deep-sea microorganisms by a two-compartment system. An open vessel suspended above an anaerobic culture allowed oxygen diffusion to the upper compartment (fig. S8A). The system's functionality was confirmed by a color change of medium from colorless to pink in the upper vessel when strains DY0037 and DY0609 were cultured in the lower compartment, demonstrating oxygen diffusion (fig. S8, B and C). Subsequent experiments showed that oxygen generated by strains DY0037 and DY0609 significantly inhibited the growth of a deep-sea strictly anaerobic methanogen (*Methanolobus* sp. ZRKC1 isolated from the deep-sea cold seep) (Fig. 3D), suggesting their potentials in reducing the production of methane and thereby affecting the methane oxidation metabolism in the deep-sea environments. On the other hand, oxygen produced by strains DY0037 and DY0609 rescued the growth of a deep-sea strictly aerobic bacterium (*Erythrobacter* strain 21-3 isolated from the deep-sea cold seep (*31*)) that cultured in the absolutely anerobic condition (Fig. 3E). With simultaneous cultivation of strain DY0037 or DY0609 inside the dialysis bag and *Erythrobacter* sp. 21-3 externally, oxygen produced by two strains was found to significantly enhance the production of zero-valent sulfur (ZVS), which was demonstrated to be an oxidation product of thiosulfate (*31*) (Fig. 3F). Thus, microbial DOP might also play a key role in deep-sea biogeochemical element cycle, particularly the element oxidation process.

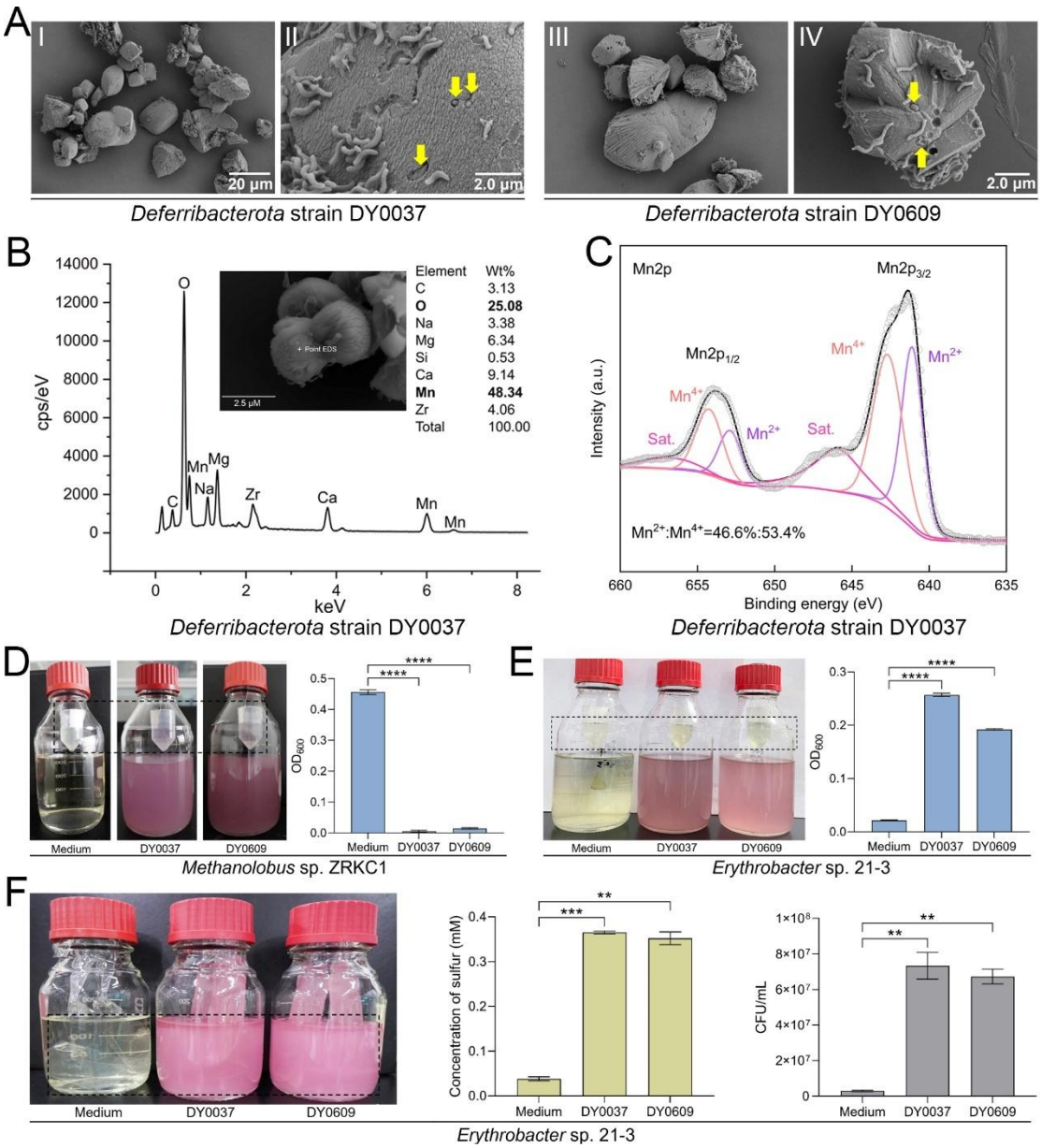

Fig. 3. *Deferribacterota* strains potentially promotes the formation of manganese nodules and impact the growth and metabolism of other deep-sea obligately anaerobic and aerobic microbes through their produced dark oxygen. (**A**) Field-emission scanning electron microscopy (FESEM) images of mineral precipitates formed by strains DY0037 and DY0609 cultured in T16 medium with 20 mM $MnCl_2$ supplementation. Yellow arrows indicate cells embedded within precipitates. (**B**) Energy dispersive spectrum (EDS) analysis of the precipitates formed by strain DY0037. (**C**) X-ray photoelectron spectroscopy (XPS) analysis of the ratio of manganese (II) to manganese (IV) ions in precipitates formed by strain DY0037. (**D**) An experimental setup in which strains DY0037 and DY0609 are cultured in an anaerobic bottle, with a deep-sea obligately anaerobic methanogen (*Methanolobus* sp. ZRKC1) inoculated in a small container suspended above,

to assess the effect of upper-layer oxygen produced by strains DY0037 and DY0609 on anaerobe's growth. (**E**) An experimental setup in which strains DY0037 and DY0609 are cultured in an anaerobic bottle, with a deep-sea obligately aerobic *Erythrobacter* sp. 21-3 inoculated in a small container suspended above, to assess the effect of upper-layer oxygen produced by strains DY0037 and DY0609 on aerobe's growth. (**F**) An experimental setup in which strains DY0037 and DY0609 are cultured within a respective dialysis bag inside an anaerobic bottle, with an obligately aerobic *Erythrobacter* sp. 21-3 inoculated outside the dialysis bag using 2216E medium supplemented with 40 mM sodium thiosulfate, to assess the effect of upper-layer oxygen produced by strains DY0037 and DY0609 on elemental sulfur production and growth of *Erythrobacter* sp. 21-3. Error bars show mean ± SD. $^{**}P < 0.01$, $^{***}P < 0.001$, $^{****}P < 0.0001$.

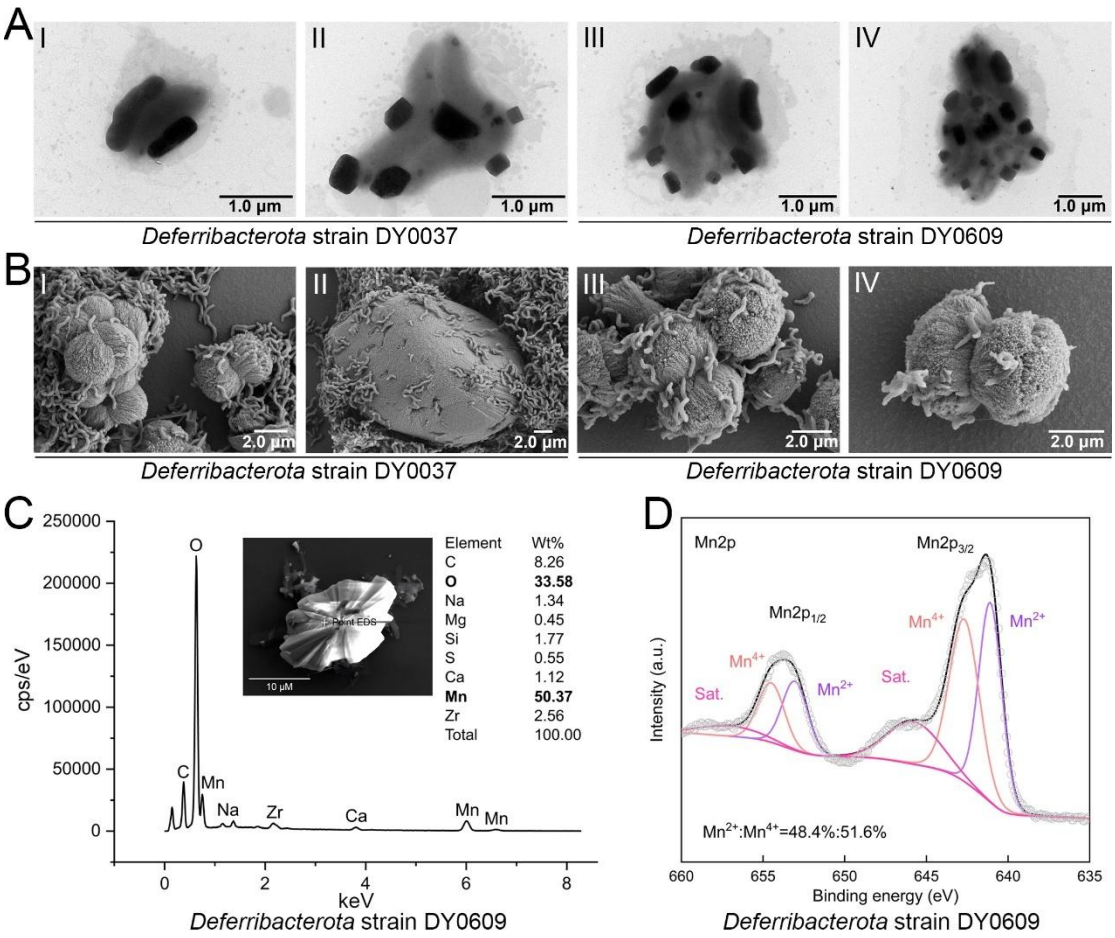

fig. S7. Microscopic and elemental composition analyses of minerals produced by *Deferribacterota* strains DY0037 and DY0609. (**A**) Transmission electron microscopy (TEM) images of strains DY0037 and DY0609 cultured in T16 medium with 20 mM $MnCl_2$

supplementation. (**B**) Field-emission scanning electron microscopy (FESEM) images of precipitates and cell morphology of strains DY0037 and DY0609 cultured in T16 medium with 20 mM $MnCl_2$ supplementation. (**C**) Energy dispersive spectrum (EDS) analysis of the precipitates formed by strain DY0609. (**D**) X-ray photoelectron spectroscopy (XPS) analysis of the ratio of manganese (II) to manganese (IV) ions in precipitate formed by strain DY0609.

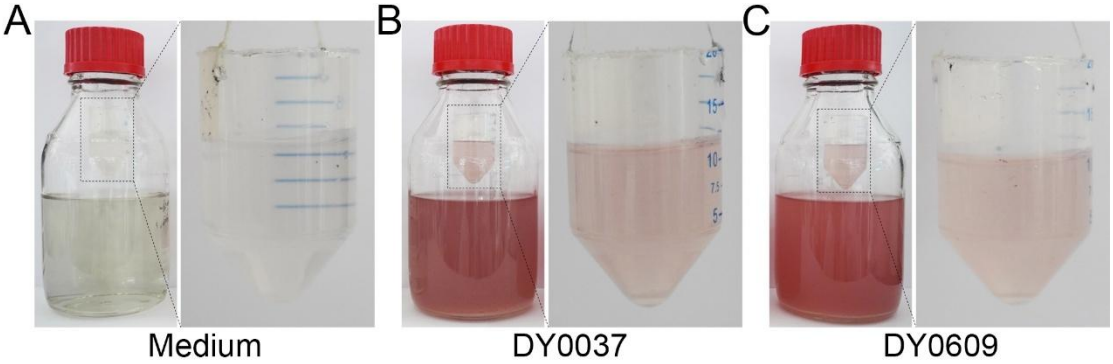

fig. S8. An experimental setup consisting of a small container suspended inside an anaerobic bottle to confirm oxygen presence in the upper layer during cultivation without (A) or with *Deferribacterota* strain DY0037 (B), or DY0609 (C).

To mimic the impacts of oxygen produced by strains DY0037 and DY0609 on the surrounding microbial community under the natural condition, we respectively cultivated two strains within the dialysis bag, and simultaneously inoculated the exterior with homogenized deep-sea sediment samples (fig. S9A). Direct plating of the enriched samples onto aerobic medium revealed a substantially higher abundance of aerobic bacteria in the presence of strains DY0037 and DY0609 compared to the control group (with blank medium inside the dialysis bag) (fig. S9B). Furthermore, amplicon sequencing analysis indicated that strains DY0037 and DY0609 enriched for a diverse range of aerobic bacteria (predominantly *Pseudomonadota*, such as *Pseudomonas*, *Vibrio*, *Shewanella*, et.), at significantly higher levels than controls, whereas control samples predominantly enriched for anaerobic bacteria (mainly members belonging to *Clostridia* and *Fusobacteriota*) (fig. S9C). The analysis of aerobic metabolism associated genes (*32*) further showed a markedly higher abundance in the experimental groups (strains DY0037 and DY0609) compared to controls (fig. S9D). These results

indicate that oxygen produced by *Deferribacterota* strains may create an oxic niche in deep-sea environments, enabling the persistence of aerobic life. This observation also offers a mechanistic explanation for the seemingly paradoxical presence of aerobic microbes in nominally anoxic environments (such as groundwater, subsurface, lake, wetland, deep sea, et.) (*4, 14*) , and suggests that similar microbial DOP processes may be common in these environments.

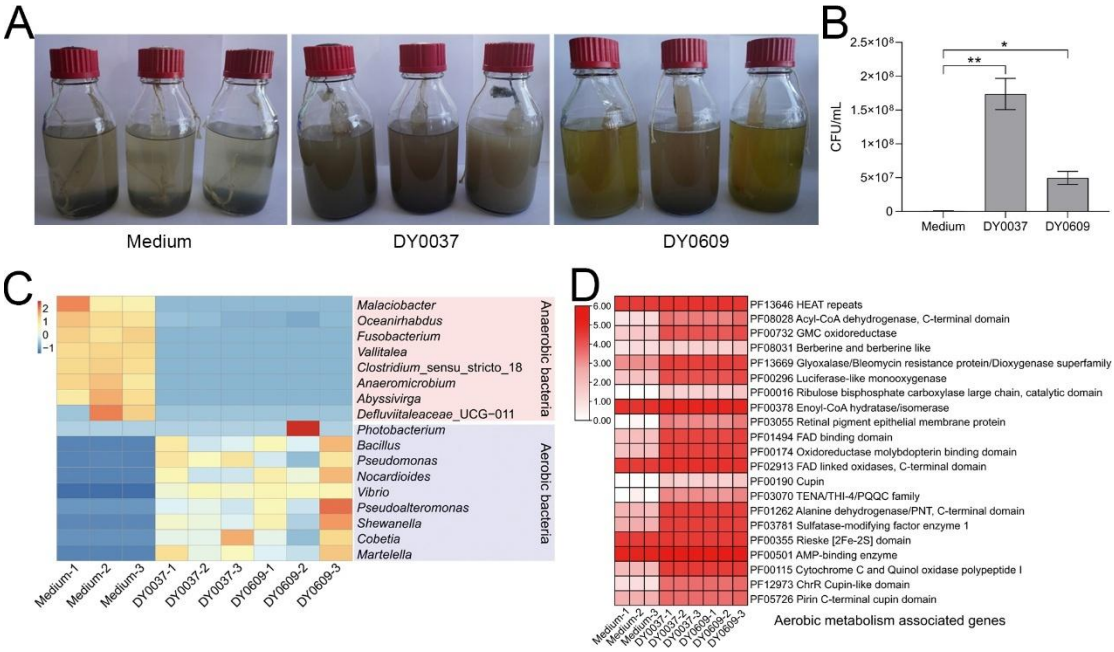

fig. S9. Effects of *Deferribacterota* strains DY0037 and DY0609 on microbial community composition and aerobic metabolism in deep-sea sediment samples. (**A**) An experimental setup in which strains DY0037 and DY0609 are cultured within a dialysis bag inside an anaerobic bottle, with an equal amount of sediment sample inoculated outside the dialysis bag, and uninoculated medium serving as the control. (**B**) Quantification of aerobic colony-forming units (CFUs) in experimental groups (strains DY0037 and DY0609) and the control group (uninoculated medium) using the plate count method. (**C**) Amplicon sequencing analysis of enriched microbial community composition (aerobes and anaerobes) in experimental groups (strains DY0037 and DY0609) and the control group (uninoculated medium). (**D**) Abundance of genes associated with aerobic metabolism in enriched microbial communities from experimental groups (strains DY0037 and DY0609) and the control group (uninoculated medium), assessed by amplicon sequencing. Error bars show mean ± SD. *$P < 0.05$, **$P < 0.01$.

Beside the aerobic microbial lives, how about the potential contribution of *Deferribacterota* DOP to animal respiration? To evaluate the support of oxygen produced by strains DY0037 and DY0609 on animal survival, we used ants (fig. S10A) and locusts (fig. S10C) as experimental organisms. We observed a significant extension of both ant and locust survival times in the presence of oxygen diffused from cultures of strains DY0037 and DY0609, with a more pronounced effect elicited by strain DY0609 (fig. S10, B and D), consistent well with its relative higher oxygen-production capability throughout the entire cultivation period (Fig. 1C). These findings demonstrate that oxygen production by strains DY0037 and DY0609 may have broad implications for both microbial and macroscopic life, suggesting potential applications in life support systems for space and deep-sea exploration. Actually, *Deferribacterota* bacteria have been shown to be dominant in the gut microbiome of blind shrimp inhabiting hydrothermal vents (*25*). The symbiotic relationship between *Deferribacterota* bacteria and animal host, evidenced by the exchange of material and energy, suggests that *Deferribacterota* bacteria function as gut symbionts (*25*). The potential for *in situ* oxygen production by this symbiont in blind shrimp, therefore, offers advantages for blind shrimp to survive in extreme environments, and provides novel perspectives to study the interaction between gut symbionts and host.

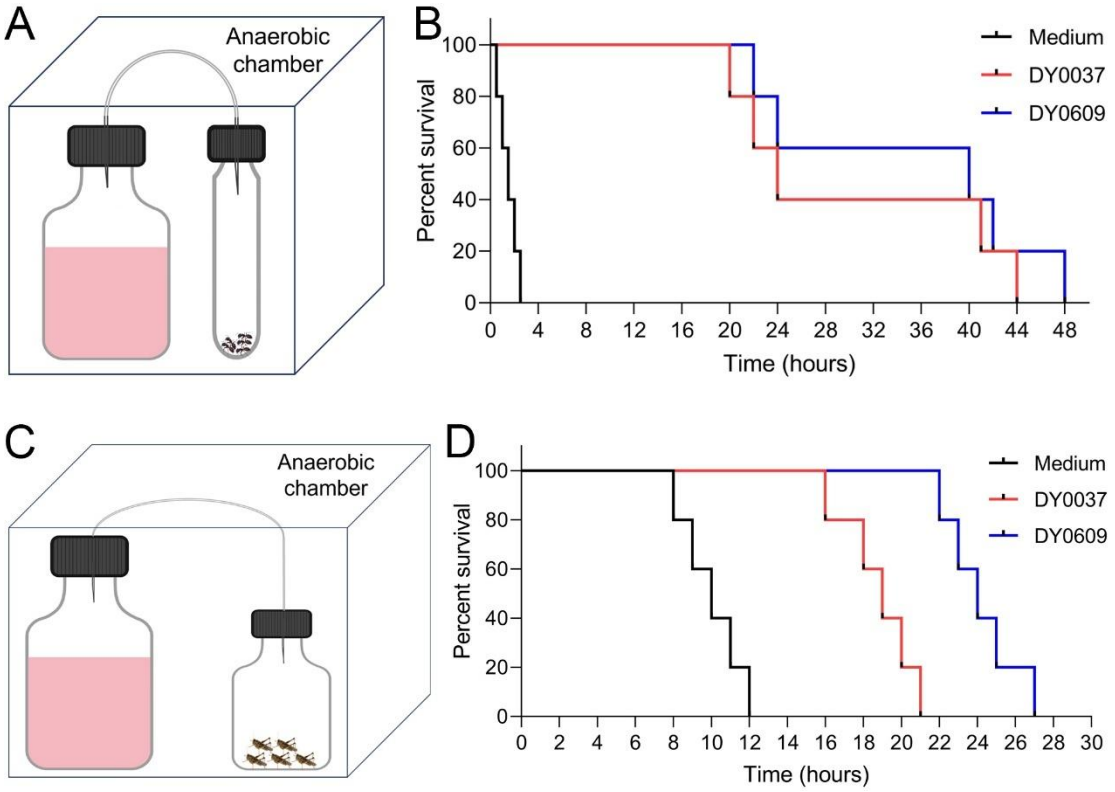

fig. S10. Supporting effect of oxygen produced by *Deferribacterota* strains DY0037 and DY0609 on insect survival when cultured in the oxygen absent container. (**A**) An experimental setup consisting of a 500 mL anaerobic bottle connected to a 15 mL anaerobic tube inside an anaerobic chamber, designed to assess the impact of oxygen produced by strains DY0037 and DY0609 on ant survival time. (**B**) Survival time assays of ants under the influence of oxygen produced by strains DY0037 and DY0609. (**C**) An experimental setup consisting of a 500 mL anaerobic bottle connected to a 250 mL anaerobic bottle inside an anaerobic chamber, designed to assess the impact of oxygen produced by strains DY0037 and DY0609 on locust survival time. (**D**) Survival time assays of locusts under the influence of oxygen produced by strains DY0037 and DY0609.

Diverse deep-sea microorganisms produce dark oxygen

To investigate the prevalence of deep-sea microbial DOP, we performed targeted enrichments from hydrothermal vent, cold seep, and seamount samples by using the nitrate-containing medium, resulting in the isolation of a diverse collection of oxygen-producing microbes. These included some *Pseudomonadota* strains DY0742 (hydrothermal vent), 24LQ007 (cold seep), and 273

(seamount), *Campylobacterota* strain DY0563 (hydrothermal vent), and *Deinococcota* strain DY0809b (hydrothermal vent). Genomic and physiological assays excluded the possibility of photosynthetic and other abiotic oxygen production in these strains, indicating their DOP capability. Further genomic analyses of the *Pseudomonadota* strains (DY0742, 24LQ007, and 273) revealed the presence of complete DNRA and denitrification pathways (Fig. 4A). During anaerobic growth of these *Pseudomonadota* strains, nitrate concentrations significantly decreased while nitrite concentrations increased, with no significant change in ammonium concentrations. Furthermore, a decrease in total inorganic nitrogen content was observed, indicating the nitrogen loss as gaseous products during denitrification (Fig. 4B and fig. S11). In addition, the dissolved oxygen concentrations in cultures of these three *Pseudomonadota* strains reached approximately 20 μM during growth. Previous studies have reported oxygen production via denitrification in *Pseudomonas* species (*20*), and combined with our findings, we propose that these deep-sea *Pseudomonadota* strains are capable of oxygen production through denitrification. To validate the DOP pathway, we generated the *norBCD* (a gene cluster potentially associated with oxygen production) deletion mutant of *Pseudomonadota* strain DY0742. Under anaerobic conditions, the wild-type strain DY0742 exhibited obvious growth, while the mutant failed to grow, whereas both strains exhibited regular growth under aerobic conditions (Fig. 4C). This indicates that *norBCD* is critical for anaerobic denitrification and oxygen production in strain DY0742, whose deletion ablates anaerobic growth.

Genomic analyses revealed that the *Campylobacterota* strain DY0563 possesses a complete DNRA pathway and an incomplete denitrification pathway (Fig. 4D), while the *Deinococcota* strain DY0809b contains an incomplete DNRA pathway and a nearly complete denitrification pathway (lacking *nosZ*) (Fig. 4F). Ion concentration analyses showed that nitrate concentrations significantly decreased while nitrite and dissolved oxygen concentrations increased during growth of both *Campylobacterota* strain DY0563 and *Deinococcota* strain DY0809b, with no substantial change in ammonium concentrations (Fig. 4, E-G). Therefore, we propose that *Campylobacterota* strain

DY0563 and *Deinococcota* strain DY0809b might generate oxygen during nitrate reduction to nitrite (Fig. 4D), with the *Deinococcota* strain DY0809b also potentially producing oxygen through a denitrification pathway similar as the *Pseudomonadota* bacteria (Fig. 4F). However, the oxygen production mechanism of these strains remains unclear, warranting further investigation to elucidate the underlying mechanism and key genes.

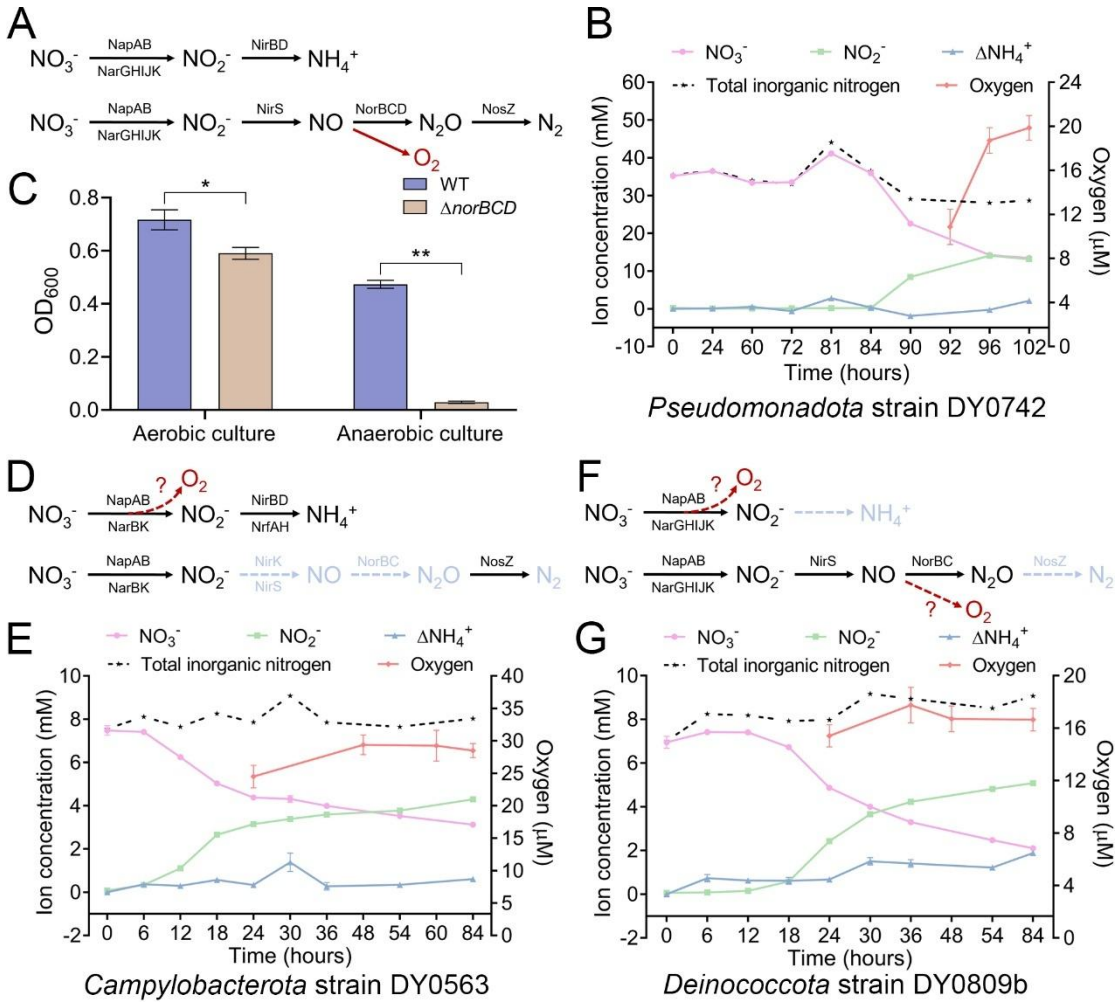

Fig. 4. Genomic and metabolic profiles of diverse deep-sea bacteria that producing dark oxygen through nitrate reduction dependent pathways. (**A, D, F**) Analysis of genes involved in DNRA and denitrification pathways and the proposed oxygen production pathway in *Pseudomonadota* strain DY0742 (**A**), *Campylobacterota* strain DY0563 (**D**), and *Deinococcota* strain DY0809b (**F**). Solid black arrows indicate the presence of relevant genes and intermediates, while dashed light blue arrows denote the absence of relevant genes and intermediates. Solid or dashed red arrow indicates the potential location of oxygen production. (**B, E, G**) Concentrations of

each inorganic nitrogen ion (NO_3^-, NO_2^-, NH_4^+), total inorganic nitrogen, and dissolved oxygen during cultivation of *Pseudomonadota* strain DY0742 (**B**), *Campylobacterota* strain DY0563 (**E**), and *Deinococcota* strain DY0809b (**G**). ΔNH_4^+ indicates the difference between the final and initial concentrations of NH_4^+ present in the culture. (**C**) Growth profile of wild-type strain DY0742 and its *norBCD* deletion mutant under aerobic and anaerobic conditions. Error bars show mean ± SD. $^*P < 0.05$, $^{**}P < 0.01$.

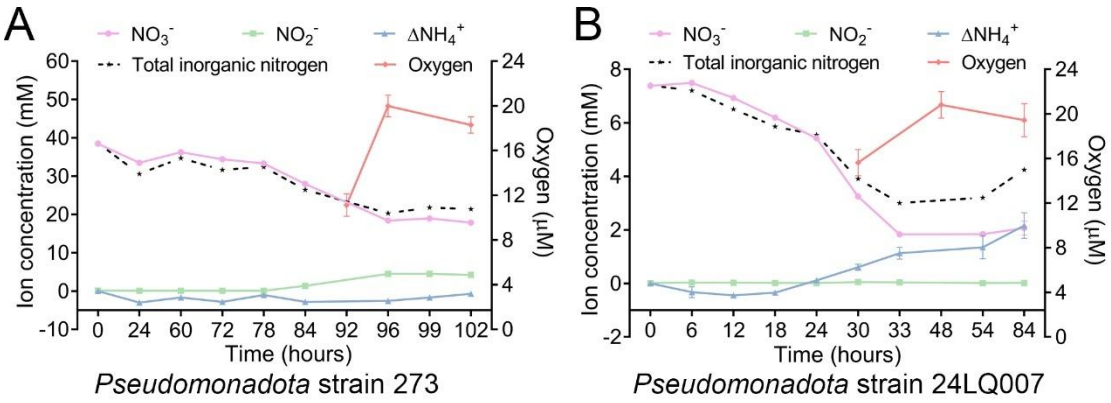

fig. S11. Dynamics of concentrations of each inorganic nitrogen ion (NO_3^-, NO_2^-, or NH_4^+), total inorganic nitrogen, and dissolved oxygen during cultivation of *Pseudomonadota* strains 273 (A) and 24LQ007 (B). ΔNH_4^+ indicates the difference between final and initial concentrations of NH_4^+ present in the culture.

Furthermore, beyond the aforementioned oxygen-producing microorganisms, we performed a comparative genomic analysis of nitrogen metabolism genes in other deep-sea microbial groups that are incapable of nitrate-dependent oxygen production. We found that microorganisms capable of producing oxygen predominantly possess genes associated with either DNRA or denitrification pathway, whereas those unable to produce oxygen via nitrate reduction largely lack these genes (fig. S12). Given the broad distribution of DNRA or denitrification pathway in many microorganisms, we infer that DOP driven by nitrate reduction may be widely distributed in diverse deep-sea environments, contributing to oxygen availability in their surrounding habitats.

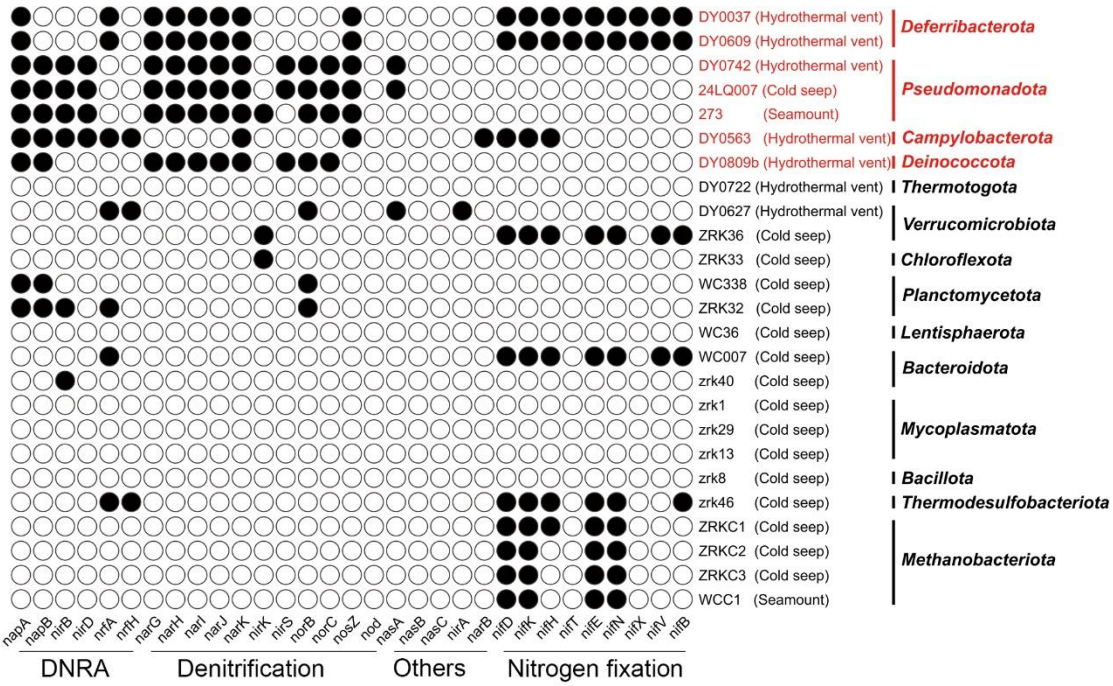

fig. S12. Distribution of nitrogen metabolism associated genes across some deep-sea microbial representatives. Statistical analysis of the distribution of nitrogen metabolism (DNRA, denitrification, nitrogen fixation, and others) associated genes across cultured deep-sea microbial representatives in our laboratory. Microbial groups capable of producing dark oxygen through nitrate reduction pathways are indicated in red, while those without this capacity are shown in black. The isolation source of corresponding strain is indicated in parentheses. Bacterial phylum name is shown after the vertical line.

Conclusions and perspectives

This study presents the cultivation of diverse deep-sea microbial groups capable of producing dark oxygen through different nitrate reduction pathways, including the identification of a novel oxygen-producing pathway coupled to DNRA in the *Deferribacterota* phylum. Our study strongly indicates that microbial DOP in deep sea closely relates to nitrate metabolism. Consistently, oxygen concentrations with depth in the deep sea (>1000 m) indeed positively correlated to available nitrate levels (*21*). Thus, microbial dark oxygen could be a significant oxygen source in nitrate-rich ocean worlds, even in the absence of light. The resulting oxygen supports the growth of the faunal community, impacts the growth and metabolism of aerobic and anaerobic

microorganisms, and shapes the geological system via promotion of the formation of polymetallic nodules (Fig. 5A). Due to the DOP capability of polymetallic nodules (*19*), the mining of them might destroy the deep-sea ecosystem, thereby limiting the exploitation of these deep-sea valuable mineral resources. Microorganisms producing dark oxygen cultured in our study would be good candidates for remediation of deep-sea ecological environments destroyed by the mining of polymetallic nodules. Moreover, deep-sea dark oxygen-producing microorganisms are potentially utilized to enhance the oxygen content of ocean oxygen minimum zones.

Within deep-sea environments, DNRA is more prevalent than denitrification among microbial communities (*33-35*). Our research on deep-sea hydrothermal vent *Deferribacterota* bacteria, which link DNRA to DOP, highlights their considerable contribution to early ocean oxygen sources. Moreover, previous findings suggest substantial atmospheric oxygen levels existed approximately 3 billion years ago, more than 600 million years before the GOE and 300-400 million years earlier than previous estimates of Earth's surface oxygenation (*36*). Since nitrogen oxides were present on early Earth, coupled with previous and our results, suggests a novel perspective on oxygen's origins (*6, 7*). Intra-aerobic denitrification and anaerobic DNRA may have either preceded photosynthetic oxygen production or provided critical niches for the evolution of aerobic pathways in the largely anaerobic environment before the GOE. Evidence from Archean and early Proterozoic geochemical records also indicates that DNRA rather than solely denitrification to N_2, may have contributed to biological nitrate utilization (37) (Fig. 5B). Therefore, both nitrate reduction-dependent oxygenic production (NRDOP) and photosynthesis-dependent oxygenic production (PDOP) are proposed to play critical roles to the rise of GOE.

Furthermore, both nitrate and chlorate are present on the Mars and Martian meteorites, including detected nitrate levels up to 1000 ppm in Martian sediments (*38, 39*), provide potential resources for life. The subsurface nitrates on Mars could act as a source of bioavailable nitrogen and oxygen, especially within its subsurface ecosystems (*40*). Here the dark oxygen-producing bacteria including *Deferribacterota*, *Deinococcota*, *Campylobacterota*, and *Pseudomonadota* strains that

isolated from deep-sea hydrothermal vents are capable of anaerobic growth and tolerate a wide temperature range. These characteristics suggest their potentials to generate dark oxygen from nitrate on Mars, thereby terraforming the Martian ecosystem and potentially facilitating human colonization in the future.

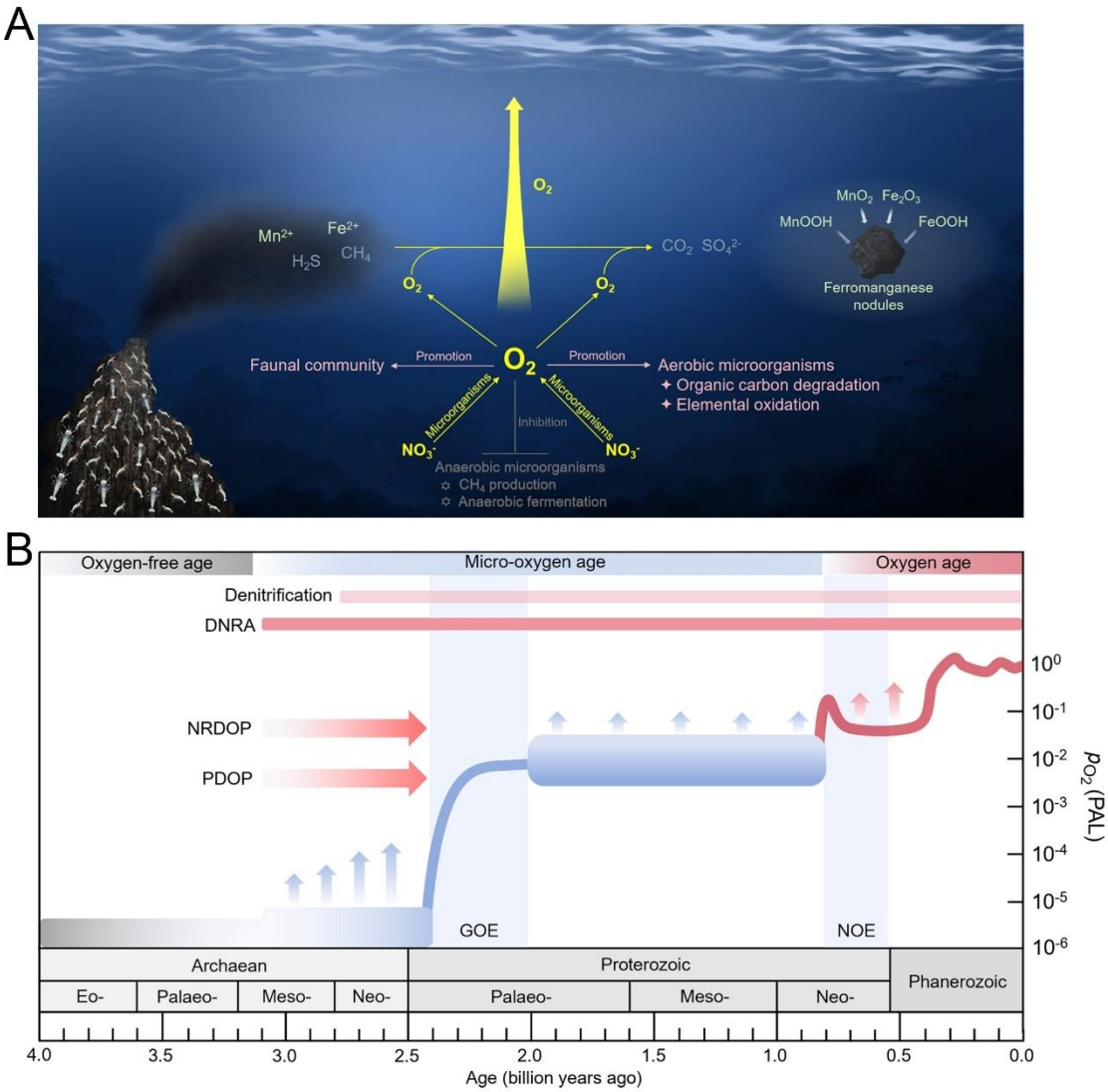

Fig. 5. The proposed models showing the contribution of microbial dark oxygen produced through nitrate reduction pathways to deep-sea ecosystems and Earth's atmospheric oxygen levels. (**A**) A schematic diagram depicting the ecological effect of dark oxygen produced by deep-sea microorganisms through nitrate reduction pathways. Yellow arrows denote the release of oxygen by deep-sea microorganisms through nitrate reduction. (**B**) A proposed model describing the contributions of different oxygen-producing pathways to the evolution of Earth's atmospheric oxygen (O_2) levels over geological time. The gray, blue, and red bands are suggested by references

(*41*) and (*42*). *p*O2 (PAL), atmospheric partial pressure of oxygen relative to the PAL. The Great Oxygenation Event (GOE; 2.5-2.4 to 2.1-2.0 billion years ago), and the Neoproterozoic Oxygenation Event (NOE; 0.8 to 0.5 billion years ago) highlight significant intervals of atmospheric oxygen rise (see references (*43*), (*44*), and (*45*) for reviews of NOE through Devonian oxygenation). The light red and red shaded boxes in the panel denote the respective timeframes for the emergence of microbial denitrification and DNRA pathways. Red arrows to the right show the approximate timing of the nitrate reduction-dependent oxygenic production (NRDOP) and photosynthesis-dependent oxygenic production (PDOP), plotted without reference to the x axes due to uncertainties in their precise ages.

Materials and methods

Enrichment and cultivation of deep-sea oxygen-producing microorganisms

The deep-sea hydrothermal vent samples were collected by ShenhaiYihao from the lost city hydrothermal field in the North Atlantic (W42°7’9.38”, N 30°7’25.92”). The deep-sea cold seep (E119°17’07.322”, N22°06’58.598”) and seamount (E110°41’12.616”, N17°22’11.438”) samples were collected by *RV KEXUE* in the South China Sea. To isolate and cultivate oxygen-producing microorganisms, these deep-sea sedimental samples were added to the 15 mL anaerobic tube containing 10 mL T13 medium (0.02 g/L Na_2SO_4, 1.0 g/L KH_2PO_4, 1.0 g/L NH_4Cl, 20.0 g/L NaCl, 3.0 g/L $MgCl_2$, 0.5 g/L KCl, 0.15 g/L $CaCl_2$, 1.0 g/L $NaNO_3$, 1.0 g/L CH_3COONa, 1.0 g/L $NaHCO_3$, 0.5 g/L fumarate, 0.5 g/L yeast extract, 0.5 g/L peptone, 1.0 g/L cysteine hydrochloride, 500 μL/L 0.1 % (w/v) resazurin, 10 mL/L trace element solution (1.5 g/L nitrilotriacetic acid, 3.0 g/L $MgSO_4{\cdot}7H_2O$, 0.5 g/L $MnSO_4{\cdot}H_2O$, 1.0 g/L NaCl, 0.1 g/L $FeSO_4{\cdot}7H_2O$, 0.18 g/L $CoSO_4{\cdot}7H_2O$, 0.1 g/L $CaCl_2{\cdot}2H_2O$, 0.18 g/L $ZnSO_4{\cdot}7H_2O$, 0.01 g/L $CuSO_4{\cdot}5H_2O$, 0.02 g/L $AlK(SO_4)_2{\cdot}12H_2O$, 0.01 g/L H_3BO_3, 0.01 g/L $Na_2MoO_4{\cdot}2H_2O$, 0.03 g/L $NiCl_2{\cdot}6H_2O$, 0.3 mg/L $Na_2SeO_3{\cdot}5H_2O$, 0.4 mg/L $Na_2WO_4{\cdot}2H_2O$, 1.0 L distilled water), 1.0 L sterilized distilled water, pH 7.0), respectively. The medium was prepared under a 100% N_2 gas phase and sterilized by autoclaving at 115 °C for 30 minutes. The inoculated media were anaerobically incubated at either 28 °C or 55 °C for one week. The T13 medium supplemented with 15 g/L agar was evenly spread onto the inside wall

of a Hungate tube, which formed a thin layer of medium for the bacteria to grow. After this, 50 μL of the enriched culture was anaerobically transferred into an anaerobic roll tube and then spread on to the medium layer. These tubes were also anaerobically cultured at either 28 °C or 55 °C for three days. Single colonies were selected using sterilized bamboo sticks; they were then cultured in the 15 mL Hungate tube containing 10 mL T13 medium at either 28 °C or 55 °C for three days. The anaerobic tubes in which the culture medium turned pink were selected and then microbial species were identified by PCR. These deep-sea microorganisms were selected and purified by repeating the Hungate roll-tube method. The purity was confirmed regularly by observation using a transmission electron microscope (TEM) and by repeating partial sequencing of the 16S rRNA gene.

TEM observation

To observe the morphological characteristics of *Deferribacterota* strains DY0037 and DY0609, 10 mL culture was collected by centrifuging at 5000 × *g* for three minutes. Cells were then washed three times with PBS buffer (137 mM NaCl, 2.7 mM KCl, 10 mM Na_2HPO_4, 1.8 mM KH_2PO_4, 1 L sterile water, pH 7.4). Finally, the cells were suspended in 20 μL PBS buffer, and then transferred onto copper grids coated with a carbon film by immersing the grids in the cell suspension for 20 minutes. All samples were examined under TEM (HT7700, Hitachi, Japan).

Genome sequencing, annotation, and analysis

For genomic sequencing, *Deferribacterota* strains DY0037 and DY0609, *Campylobacterota* strain DY0563 and *Deinococcota* strain DY0809b were incubated in QY5 medium (0.17 g/L KH_2PO_4, 3.0 g/L $NaNO_3$, 9.0 g/L NaCl, 1.0 g/L $MgCl_2$, 2.5 g/L D-Trehalose anhydrous, 0.17 g/L KCl, 0.08 g/L $CaCl_2$, 0.17 g/L NH_4Cl, 1.0 g/L $NaHCO_3$, 0.5 g/L yeast extract, 2.5 g/L peptone, 0.2 g/L cysteine hydrochloride, 500 μL/L 0.1 % (w/v) resazurin, 5 mL/L trace element solution, 0.5 L sterilized distilled water and 0.5 L sterilized seawater, pH 7.0); *Pseudomonadota* strains DY0742, 24LQ007, and 273 were incubated in T14 medium (0.02 g/L Na_2SO_4, 1.0 g/L KH_2PO_4, 1.0 g/L NH_4Cl, 20.0 g/L NaCl, 3.0 g/L $MgCl_2$, 0.5 g/L KCl, 0.15 g/L $CaCl_2$, 1.0 g/L

588 $NaNO_3$, 1.0 g/L CH_3COONa, 1.0 g/L $NaHCO_3$, 0.5 g/L fumarate, 0.5 g/L yeast extract,
589 0.5 g/L peptone, 1.0 g/L cysteine hydrochloride, 500 μL/L 0.1 % (w/v) resazurin, 10
590 mL/L trace element solution, 1.0 L sterilized distilled water, pH 7.0). Bacterial cells
591 were harvested after three days of incubation at either 28 °C (strains DY0037, DY0609,
592 DY0742, DY0828, LQ001, and 273), 37 °C (strain DY0563), or 55 °C (strain
593 DY0809b). Genomic DNA was isolated by using the PowerSoil DNA isolation kit (Mo
594 Bio Laboratories Inc., Carlsbad, CA). Thereafter, the genome sequencing was carried
595 out with both the Illumina NovaSeq PE150 (San Diego, USA) and Nanopore
596 PromethION platform (Oxford, UK) at the Beijing Novogene Bioinformatics
597 Technology Co., Ltd. A complete description of the library construction, sequencing,
598 and assembly was performed as previously described (*46*). We used seven databases to
599 predict gene functions, including Pfam (Protein Families Database,
600 http://pfam.xfam.org/), GO (Gene Ontology, http://geneontology.org/) (*47*), KEGG
601 (Kyoto Encyclopedia of Genes and Genomes, http://www.genome.jp/kegg/) (*48*), COG
602 (Clusters of Orthologous Groups, http://www.ncbi.nlm.nih.gov/COG/) (*49*), NR (Non-
603 Redundant Protein Database databases), TCDB (Transporter Classification Database),
604 and Swiss-Prot (http://www.ebi.ac.uk/uniprot/) (*50*). A whole genome Blast search (E-
605 value less than 1e-5, minimal alignment length percentage larger than 40%) was
606 performed against above seven databases.

607 **Phylogenetic analysis**

608 To construct a maximum likelihood 16S rRNA phylogenetic tree, the full-length 16S
609 rRNA gene sequences of *Deferribacterota* strains DY0037 and DY0609and other
610 related taxa were extracted from their corresponding genomes
611 (www.ncbi.nlm.nih.gov/). The phylogenetic tree was constructed using the W-IQ-
612 TREE web server (http://iqtree.cibiv.univie.ac.at) (*51*) using the "GTR+F+I+G4"
613 model, and the Interactive Tree of Life (iTOL v5) online tool (*52*) was used to edit the
614 phylogenetic trees.

615 **Measurement of bacterial growth and dissolved oxygen concentration**

616 To assess the growth and dissolved oxygen production of *Deferribacterota* strains

617 DY0037 and DY0609, T13 medium was selected. To assess the growth and dissolved
618 oxygen production of *Campylobacterota* strain DY0563 and *Deinococcota* strain
619 DY0809b, QY5 medium was selected. To assess the growth and dissolved oxygen
620 production of *Pseudomonadota* strains 24LQ007, DY0742, and 273, T14 medium was
621 selected. For each assay, 4.0 mL fresh culture of different strains was inoculated in a
622 500 mL Hungate bottle containing 400 mL of the respective media. All Hungate bottles
623 were anaerobically incubated at either 28 °C (strains DY0037, DY0609, DY0742,
624 DY0828, LQ001, and 273), 37 °C (strain DY0563), or 55 °C (strain DY0809b).
625 Bacterial growth was monitored by measuring daily OD_{600} values via a microplate
626 reader (Infinite M1000 Pro; Tecan, Mannedorf, Switzerland) until cell growth reached
627 a stationary phase. In addition, to determine the effect of nitrate on the growth of strains
628 DY0037 and DY0609, we compared its growth in T13 medium with and without
629 sodium nitrate. Three replicates were performed for each condition. The concentrations
630 of dissolved oxygen were determined using a liquid phase oxygen electrode (Hansatech,
631 Oxygraph+, UK).

632 **Experimental exclusion of alternative oxygen sources**

633 To determine the effect of seed culture components on oxygen production in
634 *Deferribacterota* strains DY0037 and DY0609, seed culture was incorporated into T13
635 medium before and after sterilization. Subsequently, growth and dissolved oxygen
636 levels were measured after two days of incubation at 28 °C. To exclude
637 H_2O_2 dismutation as a potential oxygen production mechanism, strains DY0037 and
638 DY0609 were grown in T13 medium supplemented with 0.2 mM pyruvate, as α-keto
639 acids detoxify H_2O_2 through abiotic decarboxylation (*24*). To exclude photosynthetic
640 oxygen production, strains DY0037 and DY0609 were cultivated under light and dark
641 conditions at 28 °C for two days, followed by measurements of growth and dissolved
642 oxygen levels.

643 **Transcriptomics**

644 For transcriptomic sequencing, *Deferribacterota* strains DY0037 and DY0609 were
645 cultured in 400 mL of either T13 medium supplemented with different sodium nitrate

(0.1 g/L, 0.5 g/L, 1.0 g/L, and 3.0 g/L) at 28 °C for two days. Three biological replicates were cultured for each condition. Following this, cells from three replicates were collected respectively for transcriptomic sequencing by Novogene (Tianjin, China), as previously described (*46, 53*). Briefly, RNA-seq data were generated using a NovaSeq 6000 instrument with PE150. Raw reads were trimmed for adaptors and low-quality sequences using Trimmomatic (*54*), and mRNA was recovered with SortMeRNA (*55*) (default settings) after removing tRNA and rRNA. The activity of strains DY0037 and DY0609 was evaluated using their complete circular genomes, and gene transcription levels were quantified using Burrows-Wheeler Aligner (BWA, v. 0.7.17-r1188) (*56*) to map reads, followed by SAMtools (v. 1.13) (*56*) conversion to BAM files. Read coverage was calculated with BEDTools (v. 2.30.0) (*57*), normalized to genome length, and gene expression was quantified using Fragments Per Kilobase Million (FPKM). The transcribed rank of genes was then calculated based on $\log_2$[FPKM] values.

Verification of oxygen production from nitrate via the stable isotope assay

To investigate whether the oxygen originated from nitrate, *Deferribacterota* strains DY0037 and DY0609 were cultured in T13 medium containing 10 mM ^{18}O-labeled KNO_3 instead of 1.0 g/L $NaNO_3$. After 3 days of incubation, the headspace gas was collected for gas detection and analysis ($^{18}O_2$ and $^{16}O_2$) by the isotope mass spectrometer (Delta Q, Thermo Fisher, USA).

Ion concentration detection

To quantify the ion concentrations (NO_3^-, NO_2^-, and NH_4^+) during growth of *Deferribacterota* strains DY0037 and DY0609 in T13 medium, culture supernatants were collected by centrifuging at 12000 × *g* for ten minutes every 12 hours for four days. To detect the ion concentrations (NO_3^-, NO_2^-, and NH_4^+) during growth of other bacteria (*Campylobacterota* strain DY0563, *Deinococcota* strain DY0809b, and *Pseudomonadota* strain 24LQ007 for QY5 medium, *Pseudomonadota* strains DY0742 and 273 for T14 medium), all culture supernatants were respectively collected for 84 or 102 hours. Following this, these supernatants were measured by the continuous flow analyzer (QuAAtro39, Seal, Germany).

Verification of NO_2^-/NH_4^+ production from nitrate via the stable isotope assay

To test whether nitrate can produce ammonium through DNRA pathway, *Deferribacterota* strains DY0037 and DY0609 were cultured in T13 medium containing 10 mM ^{15}N-labeled KNO_3 instead of 1.0 g/L $NaNO_3$. After 3 days of incubation, the culture supernatants were collected for detection and analysis by the Gas Isotope Ratio Mass Spectrometer (MAT 253, Thermo Fisher, USA).

X-ray diffraction (XRD) assay

To determine the mineral composition generated by *Deferribacterota* strains DY0037 and DY0609 during their growth phase, we harvested 2 g mineral particles from strains DY0037 and DY0609, respectively. These particles were washed three times with distilled water and then thoroughly dried. The XRD analysis of these dried crystal powders was performed using a Rigaku SmartLab diffractometer (SmartLab 9KW, Rigaku Corporation，Japan) at 9 kW, 45 kV, 200 mA, with a step size of 0.02, a scanning speed of 20°/min, and a 2θ range of 5-80°. Data were analyzed using MDI Jade9 and PDF-2 (release 2020), with plotting done using GraphPad Prism (release 8.0.2).

Effects of microbial dark oxygen on deep-sea microorganisms

To investigate whether oxygen produced by *Deferribacterota* strains DY0037 and DY0609 affects the growth of deep-sea microorganisms, we designed a specialized setup consisting of an open centrifuge tube containing various media placed within the 500 mL anaerobic bottle. *Deferribacterota* strains DY0037 and DY0609 were first cultured in the 500 mL anaerobic bottles containing 300 mL of T13 medium for two days. Subsequently, deep-sea microorganisms were inoculated into the upper open centrifuge tube containing different media (*Methanolobus* sp. ZRKC1 in M1 medium (1.0 g/L NH_4Cl, 1.0 g/L CH_3COONa, 1.0 g/L $NaHCO_3$, 1.0 g/L yeast extract, 1.0 g/L peptone, 1.0 g/L cysteine hydrochloride, 500 μL/L 0.1 % (w/v) resazurin, 10 mL/L methanol, 1.0 L filtered seawater, pH 7.0), *Erythrobacter* sp. 21-3 in 2216E (5.0 g/L peptone, 1.0 g/L yeast extract, 1.0 g/L cysteine hydrochloride, 500 μL/L 0.1 % (w/v) resazurin, 1.0 L filtered seawater, pH 7.0) or 2216E supplemented with 40 mM $Na_2S_2O_3$). After three days of static incubation, OD_{600} was measured via the microplate

reader.

To quantify zero-valent sulfur (ZVS) produced by *Erythrobacter* sp. 21-3 under anaerobic conditions in 2216E medium supplemented with 40 mM $Na_2S_2O_3$, we extracted ZVS from the culture using a previously described trichloromethane-based method (*58-60*). Specifically, we performed a two-step extraction, twice treating 2 mL of the culture with 5 mL of trichloromethane. The extracts were then measured using a UV–Vis spectrometer (Infinite M1000 Pro; Tecan, Männedorf, Switzerland) at 270 nm. In addition, the formation of ZVS by *Erythrobacter* sp. 21-3 resulted in high culture turbidity, compromising optical density (OD_{600}) measurements for growth monitoring. Therefore, we quantified growth by colony-forming units (CFU) after serial dilution and plating on 2216E agar, followed by a 3-day incubation.

Detection of anaerobic manganese oxidation and nodule formation

To assess the contribution of oxygen generated by *Deferribacterota* strains DY0037 and DY0609 to manganese nodule formation, two strains were cultured in T16 medium (0.02 g/L Na_2SO_4, 0.05 g/L KH_2PO_4, 0.05 g/L Na_2SiO_3, 1.0 g/L NH_4Cl, 20.0 g/L NaCl, 3.0 g/L $MgCl_2$, 0.5 g/L KCl, 0.15 g/L $CaCl_2$, 1.0 g/L $NaNO_3$, 1.0 g/L CH_3COONa, 1.0 g/L $NaHCO_3$, 1.0 g/L cysteine hydrochloride, 500 μL/L 0.1 % (w/v) resazurin, 10 mL/L trace element solution, 1.0 L sterilized distilled water, pH 7.0) supplemented with 20 mM $MnCl_2$ at 28 °C for 4 days. The resulting precipitates were then collected and analyzed using TEM and field emission scanning electron microscopy (FESEM, ZEISS, Gemini500, Germany). The energy dispersive spectrum (EDS, Ultim Max 40, Oxford Instruments, Kingdom) equipment with FESEM was used to analyze the elemental composition and content. X-ray photoelectron spectroscopy (XPS, ESCALAB 250Xi, Thermo Fisher, USA) was used to determine the ratios of different manganese oxidation states.

Amplification sequencing analysis

To investigate the potential impact of oxygen produced by *Deferribacterota* strains DY0037 and DY0609 on surrounding microbial communities, we deployed dialysis bags containing 100 mL of T13 medium inoculated with strains DY0037 and DY0609

(served as the experimental groups) or without bacteria (served as the control group) within 500 mL anaerobic bottles. These bottles also contained 350 mL of T13 medium and a homogenous suspension of deep-sea hydrothermal vent sediment, respectively. Three biological replicates were cultured for each condition. Following a 7-day static incubation at 28 °C, cells were harvested from all bottles for operational taxonomic units (OTUs) sequencing performed by Novogene (Tianjin, China). Total DNAs from these samples were extracted by the CTAB/SDS method (*61*) and were diluted to 1 ng/μL with sterile water and used for PCR template. 16S rRNA genes of distinct regions (16S V3/V4) were amplified using specific primers (341F: 5'-CCTAYGGGRBGCASCAG - 3' and 806R: 5'- GGACTACNNGGGTATCTAAT- 3') with the barcode. These PCR products were purified with a Qiagen Gel Extraction Kit (Qiagen, Germany) and prepared to construct libraries. Sequencing libraries were generated using TruSeq® DNA PCR-Free Sample Preparation Kit (Illumina, USA) following the manufacturer's instructions. The library quality was assessed on the Qubit@ 2.0 Fluorometer (Thermo Scientific) and Agilent Bioanalyzer 2100 system. And then the library was sequenced on an Illumina NovaSeq platform and 250 bp paired-end reads were generated. Paired-end reads were merged using FLASH (V1.2.7, http://ccb.jhu.edu/software/FLASH/) (*62*), which was designed to merge paired-end reads when at least some of the reads overlap those generated from the opposite end of the same DNA fragments, and the splicing sequences were called raw tags. Quality filtering on the raw tags were performed under specific filtering conditions to obtain the high-quality clean tags (*63*) according to the QIIME (V1.9.1, http://qiime.org/scripts/split_libraries_fastq.html) quality controlled process. The tags were compared with the reference database (Silva database, https://www.arb-silva.de/) using UCHIME algorithm (UCHIME Algorithm, http://www.drive5.com/usearch/manual/uchime_algo.html) (*64*) to detect chimera sequences, and then the chimera sequences were removed (*64*). And sequences analyses were performed by Uparse software (Uparse v7.0.1001, http://drive5.com/uparse/) (*65*). Sequences with ≥97% similarity were assigned to the same OTUs. The representative sequence for each OTU was screened for further annotation. For each representative

sequence, the Silva Database (release 111, 2012-07, http://www.arb-silva.de/) (*66*) was used based on Mothur algorithm to annotate taxonomic information.

Growth assays of animals in the presence of microbial dark oxygen

To assess whether the oxygen produced by *Deferribacterota* strains DY0037 and DY0609 can extend animal survival time, we conducted experiments using ants and locusts. For the ant survival experiment, *Deferribacterota* strains DY0037 and DY0609 were cultured for two days in the 250 mL anaerobic bottles containing 200 mL of T13 medium. The control group contained only T13 medium without bacterial inoculation. Five ants were placed in each 15 mL anaerobic tube, and the anaerobic bottle connected with the anaerobic tube using blood collection needle. For the locust survival experiment, *Deferribacterota* strains DY0037 and DY0609 were cultured for two days in the 500 mL anaerobic bottles containing 400 mL of T13 medium. The control group contained only T13 medium without bacterial inoculation. Five locusts were placed in each 250 mL anaerobic bottle, and the 500 mL-anaerobic bottle connected with the 250 mL-anaerobic bottle using blood collection needle. All experimental procedures and device handling were conducted within an anaerobic chamber. Finally, the survival time of each ant and locust was recorded.

Gene deletion in the *Pseudomonadota* strain DY0742

To generate a *norBCD* deletion mutant of *Pseudomonadota* strain DY0742, we amplified chromosomal fragments using primers listed in Table S1. Purified PCR products were ligated into the suicide vector pEX18Gm, incorporating an *oriT* for conjugation. The resulting plasmid was transformed successively into *E. coli* SY327 and *E. coli* S17-1 by the $CaCl_2$ method. Mating between strains DY0742 and *E. coli* S17-1 containing plasmid was performed at 28 °C for 48 hours. Colonies growing on LB agar amended with Cm (25 μg/mL) and Gm (25 μg/mL) were single-event positive recombinant strains. The individual colony was picked and incubated overnight at 28 °C with shaking in LB broth with Cm (25 μg/mL) and Gm (25 μg/mL), then diluted 1:1000 into fresh LB broth and plated onto LB agar plate amended with 10% sucrose and incubated for 48 hours at 28 °C. A single colony was re-streaked several times before

being replicated onto a LB agar plate amended with Gm (25 μg/mL) to confirm sensitivity to gentamicin and loss of the pEX18GM vector. All double recombination mutant candidates were verified by PCR amplification and sequencing. Subsequently, wild-type strain DY0742 and its *norBCD* mutant were cultured in T13 medium under both anaerobic and aerobic conditions at 28 °C for two days, OD_{600} was measured via the microplate reader.

Genomic analysis of nitrogen metabolism genes in deep-sea microorganisms

To investigate the relationship between oxygen production and nitrogen metabolism in deep-sea microorganisms, we analyzed some genomes of currently available deep-sea pure cultures (from our lab) by the above seven databases (Pfam, GO, KEGG, COG, NR, TCDB, and Swiss-Prot). The distribution of genes involved in dissimilatory nitrate reduction, denitrification, nitrogen fixation, and other nitrogen metabolism was quantified and compared in deep-sea bacterial isolates with or without oxygen production capability.

Data availability

The full-length 16S rRNA gene sequences of deep-sea bacterial strains DY0037, DY0609, DY0563, DY0809b, DY0742, 24LQ007, and 273 have been deposited at GenBank under the accession numbers PV030186, PV030187, PQ827512, PQ827461, PQ827347, PQ827449, and KU529971, respectively. The complete genome sequences of bacterial strains DY0037, DY0609, DY0563, DY0809b, DY0742, 24LQ007, and 273 have been deposited at GenBank under the accession numbers CP179913, CP179935, CP179914, CP179936, CP179937, CP179938, and CP015641, respectively. The raw sequencing reads from the transcriptomics analyses of DY0037 and DY0609 strains cultured in T13 medium supplemented with different sodium nitrate have been deposited into the NCBI Short Read Archive (accession numbers: PRJNA1216325 and PRJNA1218497, respectively). The raw sequencing reads from the amplification sequencing analyses of strains DY0037 and DY0609 have been deposited into the NCBI Short Read Archive (accession number: PRJNA1218488).

Statistical analysis

All data were expressed as means ± SD. Statistical analysis was performed using GraphPad Prism 8.0.2. Independent-sample *t*-test and single-sample *t*-test were conducted to determine the significance between groups. Differences of $P < 0.05$ were considered statistically significant (*$P < 0.05$, **$P < 0.01$, ***$P < 0.001$, ****$P < 0.0001$). Differences of $P > 0.05$ were considered not significant (ns).

Acknowledgements

This work was funded by the NSFC Innovative Group Grant (No. 42221005), Major Research Plan of the National Natural Science Foundation (Grant No. 92351301), Science and Technology Innovation Project of Laoshan Laboratory (Grant Nos. LSKJ202203103 and 2022QNLM030004-3), Shandong Provincial Natural Science Foundation (Grant Nos. ZR2024ZD49 and ZR2021ZD28), and Taishan Scholars Program (Grant Nos. tstp20230637 and tsqn202312264). We are grateful to all scientist and crew member of ShenhaiYihao and the pilots of HOV Jiaolong during the cruise of DY83 for the sample collection. We extend special appreciation to the captain and crew of the *RV KEXUE*, as well as the FAXIAN ROV team for assistance with sample collection.

Author contributions

RZ, CW, and CS conceived and designed the study; RZ and CW conducted most of the experiments; CW, HW, and HQ collected the samples from the deep-sea hydrothermal vents, cold seeps and seamounts; RZ, CW, and CS lead the writing of the paper; all authors contributed to and reviewed the paper.

References and Notes

1. N. Nelson, A. Ben-Shem, The complex architecture of oxygenic photosynthesis. *Nat. Rev. Mol. Cell Biol.* **5**, 971-982 (2004).
2. W. W. Fischer, J. Hemp, J. E. Johnson, Evolution of Oxygenic Photosynthesis. *Annu. Rev. Earth Planet. Sci.* **44**, 647-683 (2016).
3. S. E. Ruff, L. Schwab, E. Vidal, J. D. Hemingway, B. Kraft, R. Murali, Widespread occurrence of dissolved oxygen anomalies, aerobic microbes, and oxygen-producing metabolic pathways in apparently anoxic environments. *FEMS Microbiol. Ecol.* **100**, fiae132 (2024).
4. S. E. Ruff, P. Humez, I. H. de Angelis, M. Diao, M. Nightingale, S. Cho, L. Connors, O. O. Kuloyo, A. Seltzer, S. Bowman, S. D. Wankel, C. N. McClain, B. Mayer, M.

Strous, Hydrogen and dark oxygen drive microbial productivity in diverse groundwater ecosystems. *Nat. Commun.* **14**, 3194 (2023).

5. C. G. van Ginkel, G. B. Rikken, A. G. Kroon, S. W. Kengen, Purification and characterization of chlorite dismutase: a novel oxygen-generating enzyme. *Arch. Microbiol.* **166**, 321-326 (1996).
6. K. F. Ettwig, M. K. Butler, D. Le Paslier, E. Pelletier, S. Mangenot, M. M. Kuypers, F. Schreiber, B. E. Dutilh, J. Zedelius, D. de Beer, J. Gloerich, H. J. Wessels, T. van Alen, F. Luesken, M. L. Wu, K. T. van de Pas-Schoonen, H. J. Op den Camp, E. M. Janssen-Megens, K. J. Francoijs, H. Stunnenberg, J. Weissenbach, M. S. Jetten, M. Strous, Nitrite-driven anaerobic methane oxidation by oxygenic bacteria. *Nature* **464**, 543-548 (2010).
7. B. Kraft, N. Jehmlich, M. Larsen, L. A. Bristow, M. Könneke, B. Thamdrup, D. E. Canfield, Oxygen and nitrogen production by an ammonia-oxidizing archaeon. *Science* **375**, 97-100 (2022).
8. P. Dershwitz, N. L. Bandow, J. Yang, J. D. Semrau, M. T. McEllistrem, R. A. Heinze, M. Fonseca, J. C. Ledesma, J. R. Jennett, A. M. DiSpirito, N. S. Athwal, M. S. Hargrove, T. A. Bobik, H. Zischka, A. A. DiSpirito, Oxygen generation via water splitting by a novel biogenic metal Ion-binding compound. *Appl. Environ. Microbiol.* **87**, e0028621 (2021).
9. J. Xu, N. Sahai, C. M. Eggleston, M. A. A. Schoonen, Reactive oxygen species at the oxide/water interface: Formation mechanisms and implications for prebiotic chemistry and the origin of life. *Earth Planet. Sci. Lett.* **363**, 156-167 (2013).
10. K. M. Sutherland, J. D. Hemingway, D. T. Johnston, The influence of reactive oxygen species on “respiration” isotope effects. *Geochim. Cosmochim. Acta* **324**, 86-101 (2022).
11. Z. Stępniewska, A. Pytlak, A. Kuźniar, Distribution of the methanotrophic bacteria in the Western part of the Upper Silesian Coal Basin (Borynia-Zofiówka and Budryk coal mines). *Int. J. Coal Geol.* **130**, 70-78 (2014).
12. R. J. Hicks, J. K. Fredrickson, Aerobic metabolic potential of microbial populations indigenous to deep subsurface environments. *Geomicrobiol. J.* **7**, 67-78 (1989).
13. M. Pester, M. W. Friedrich, B. Schink, A. Brune, pmoA-based analysis of methanotrophs in a littoral lake sediment reveals a diverse and stable community in a dynamic environment. *Appl. Environ. Microbiol.* **70**, 3138-3142 (2004).
14. R. He, J. Wang, J. W. Pohlman, Z. Jia, Y. X. Chu, M. J. Wooller, M. B. Leigh, Metabolic flexibility of aerobic methanotrophs under anoxic conditions in Arctic lake sediments. *ISME J.* **16**, 78-90 (2022).
15. C. Graef, A. G. Hestnes, M. M. Svenning, P. Frenzel, The active methanotrophic community in a wetland from the High Arctic. *Environ. Microbiol. Rep.* **3**, 466-472 (2011).
16. J. Sarkar, M. Mondal, S. Bhattacharya, S. Dutta, S. Chatterjee, N. Mondal, S. N, A. Peketi, A. Mazumdar, W. Ghosh, Extremely oligotrophic and complex-carbon-degrading microaerobic bacteria from Arabian Sea oxygen minimum zone sediments. *Arch. Microbiol.* **206**, 179 (2024).

17. S. E. Ruff, J. F. Biddle, A. P. Teske, K. Knittel, A. Boetius, A. Ramette, Global dispersion and local diversification of the methane seep microbiome. *Proc. Natl. Acad. Sci. U. S. A.* **112**, 4015-4020 (2015).
18. S. E. Ruff, J. Felden, H. R. Gruber-Vodicka, Y. Marcon, K. Knittel, A. Ramette, A. Boetius, In situ development of a methanotrophic microbiome in deep-sea sediments. *ISME J.* **13**, 197-213 (2019).
19. A. K. Sweetman, A. J. Smith, D. S. W. de Jonge, T. Hahn, P. Schroedl, M. Silverstein, C. Andrade, R. L. Edwards, A. J. M. Lough, C. Woulds, W. B. Homoky, A. Koschinsky, S. Fuchs, T. Kuhn, F. Geiger, J. J. Marlow, Evidence of dark oxygen production at the abyssal seafloor. *Nat. Geosci.* **17**, 737-739 (2024).
20. M. Lichtenberg, L. Line, V. Schrameyer, T. H. Jakobsen, M. L. Rybtke, M. Toyofuku, N. Nomura, M. Kolpen, T. Tolker-Nielsen, M. Kühl, T. Bjarnsholt, P. Jensen, Nitric-oxide-driven oxygen release in anoxic *Pseudomonas aeruginosa*. *iScience* **24**, 103404 (2021).
21. W. Martens-Habbena, W. Qin, Archaeal nitrification without oxygen. *Science* **375**, 27-28 (2022).
22. J. S. Berg, S. Ahmerkamp, P. Pjevac, B. Hausmann, J. Milucka, M. M. M. Kuypers, How low can they go? Aerobic respiration by microorganisms under apparent anoxia. *FEMS Microbiol. Rev.* **46**, fuac006 (2022).
23. R. J. Diaz, R. Rosenberg, Spreading dead zones and consequences for marine ecosystems. *Science* **321**, 926-929 (2008).
24. J. G. Kim, S. J. Park, J. S. Sinninghe Damsté, S. Schouten, W. I. Rijpstra, M. Y. Jung, S. J. Kim, J. H. Gwak, H. Hong, O. J. Si, S. Lee, E. L. Madsen, S. K. Rhee, Hydrogen peroxide detoxification is a key mechanism for growth of ammonia-oxidizing archaea. *Proc. Natl. Acad. Sci. U. S. A.* **113**, 7888-7893 (2016).
25. L. Qi, M. Shi, F. C. Zhu, C. A. Lian, L. S. He, Genomic evidence for the first symbiotic *Deferribacterota*, a novel gut symbiont from the deep-sea hydrothermal vent shrimp *Rimicaris kairei*. *Front. Microbiol.* **14**, 1179935 (2023).
26. L. Qi, C. A. Lian, F. C. Zhu, M. Shi, L. S. He, Comparative analysis of intestinal microflora between two developmental stages of *Rimicaris kairei*, a hydrothermal shrimp from the Central Indian Ridge. *Front. Microbiol.* **12**, 802888 (2021).
27. M. L. Miroshnichenko, A. I. Slobodkin, N. A. Kostrikina, S. L'Haridon, O. Nercessian, S. Spring, E. Stackebrandt, E. A. Bonch-Osmolovskaya, C. Jeanthon, *Deferribacter abyssi* sp. nov., an anaerobic thermophile from deep-sea hydrothermal vents of the Mid-Atlantic Ridge. *Int. J. Syst. Evol. Microbiol.* **53**, 1637-1641 (2003).
28. S. Spring, M. Rohde, B. Bunk, C. Spröer, S. E. Will, M. Neumann-Schaal, New insights into the energy metabolism and taxonomy of *Deferribacteres* revealed by the characterization of a new isolate from a hypersaline microbial mat. *Environ. Microbiol.* **24**, 2543-2575 (2022).
29. J. R. Hein, A. Koschinsky, T. Kuhn, Deep-ocean polymetallic nodules as a resource for critical materials. *Nat. Rev. Earth Environ.* **1**, 158-169 (2020).

30. D. Zhang, X. Li, Y. Wu, X. Xu, Y. Liu, B. Shi, Y. Peng, D. Dai, Z. Sha, J. Zheng, Microbe-driven elemental cycling enables microbial adaptation to deep-sea ferromanganese nodule sediment fields. *Microbiome* **11**, 160 (2023).
31. J. Zhang, R. Liu, S. Xi, R. Cai, X. Zhang, C. Sun, A novel bacterial thiosulfate oxidation pathway provides a new clue about the formation of zero-valent sulfur in deep sea. *ISME J.* **14**, 2261-2274 (2020).
32. J. Jabłońska, D. S. Tawfik, The evolution of oxygen-utilizing enzymes suggests early biosphere oxygenation. *Nat. Ecol. Evol.* **5**, 442-448 (2021).
33. C. Vetriani, M. D. Speck, S. V. Ellor, R. A. Lutz, V. Starovoytov, *Thermovibrio ammonificans* sp. nov., a thermophilic, chemolithotrophic, nitrate-ammonifying bacterium from deep-sea hydrothermal vents. *Int. J. Syst. Evol. Microbiol.* **54**, 175-181 (2004).
34. I. Pérez-Rodríguez, A. Grosche, L. Massenburg, V. Starovoytov, R. A. Lutz, C. Vetriani, *Phorcysia thermohydrogeniphila* gen. nov., sp. nov., a thermophilic, chemolithoautotrophic, nitrate-ammonifying bacterium from a deep-sea hydrothermal vent. *Int. J. Syst. Evol. Microbiol.* **62**, 2388-2394 (2012).
35. C. Vetriani, J. W. Voordeckers, M. Crespo-Medina, C. E. O'Brien, D. Giovannelli, R. A. Lutz, Deep-sea hydrothermal vent *Epsilonproteobacteria* encode a conserved and widespread nitrate reduction pathway (Nap). *ISME J.* **8**, 1510-1521 (2014).
36. S. A. Crowe, L. N. Døssing, N. J. Beukes, M. Bau, S. J. Kruger, R. Frei, D. E. Canfield, Atmospheric oxygenation three billion years ago. *Nature* **501**, 535-538 (2013).
37. C. Parsons, E. E. Stüeken, C. J. Rosen, K. Mateos, R. E. Anderson, Radiation of nitrogen-metabolizing enzymes across the tree of life tracks environmental transitions in Earth history. *Geobiology* **19**, 18-34 (2021).
38. S. P. Kounaves, B. L. Carrier, G. D. O'Neil, S. T. Stroble, M. W. Claire, Evidence of martian perchlorate, chlorate, and nitrate in Mars meteorite EETA79001: Implications for oxidants and organics. *Icarus* **229**, 206-213 (2014).
39. J. C. Stern, B. Sutter, C. Freissinet, R. Navarro-González, C. P. McKay, P. D. Archer, Jr., A. Buch, A. E. Brunner, P. Coll, J. L. Eigenbrode, A. G. Fairen, H. B. Franz, D. P. Glavin, S. Kashyap, A. C. McAdam, D. W. Ming, A. Steele, C. Szopa, J. J. Wray, F. J. Martín-Torres, M. P. Zorzano, P. G. Conrad, P. R. Mahaffy, Evidence for indigenous nitrogen in sedimentary and aeolian deposits from the Curiosity rover investigations at Gale crater, Mars. *Proc. Natl. Acad. Sci. U. S. A.* **112**, 4245-4250 (2015).
40. J. R. Michalski, T. C. Onstott, S. J. Mojzsis, J. Mustard, Q. H. S. Chan, P. B. Niles, S. S. Johnson, The Martian subsurface as a potential window into the origin of life. *Nat. Geosci.* **11**, 21-26 (2018).
41. T. W. Lyons, C. T. Reinhard, N. J. Planavsky, The rise of oxygen in Earth's early ocean and atmosphere. *Nature* **506**, 307-315 (2014).
42. L. R. Kump, The rise of atmospheric oxygen. *Nature* **451**, 277-278 (2008).
43. R. Wood, A. G. Liu, F. Bowyer, P. R. Wilby, F. S. Dunn, C. G. Kenchington, J. F. H. Cuthill, E. G. Mitchell, A. Penny, Integrated records of environmental change and evolution challenge the Cambrian Explosion. *Nat. Ecol. Evol.* **3**, 528-538 (2019).

44. M. W. Wallace, A. v. Hood, A. Shuster, A. Greig, N. J. Planavsky, C. P. Reed, Oxygenation history of the Neoproterozoic to early Phanerozoic and the rise of land plants. *Earth Planet. Sci. Lett.* **466**, 12-19 (2017).
45. L. M. Och, G. A. Shields-Zhou, The Neoproterozoic oxygenation event: Environmental perturbations and biogeochemical cycling. *Earth-Sci. Rev.* **110**, 26-57 (2012).
46. R. Zheng, R. Liu, Y. Shan, R. Cai, G. Liu, C. Sun, Characterization of the first cultured free-living representative of *Candidatus* Izemoplasma uncovers its unique biology. *ISME J.* **15**, 2676-2691 (2021).
47. M. Ashburner, C. A. Ball, J. A. Blake, D. Botstein, H. Butler, J. M. Cherry, A. P. Davis, K. Dolinski, S. S. Dwight, J. T. Eppig, M. A. Harris, D. P. Hill, L. Issel-Tarver, A. Kasarskis, S. Lewis, J. C. Matese, J. E. Richardson, M. Ringwald, G. M. Rubin, G. Sherlock, Gene ontology: tool for the unification of biology. The Gene Ontology Consortium. *Nat. Genet.* **25**, 25-29 (2000).
48. M. Kanehisa, S. Goto, S. Kawashima, Y. Okuno, M. Hattori, The KEGG resource for deciphering the genome. *Nucleic Acids Res.* **32**, D277-D280 (2004).
49. M. Y. Galperin, K. S. Makarova, Y. I. Wolf, E. V. Koonin, Expanded microbial genome coverage and improved protein family annotation in the COG database. *Nucleic Acids Res.* **43**, D261-D269 (2015).
50. A. Bairoch, R. Apweiler, The SWISS-PROT protein sequence database and its supplement TrEMBL in 2000. *Nucleic Acids Res.* **28**, 45-48 (2000).
51. J. Trifinopoulos, L. T. Nguyen, A. von Haeseler, B. Q. Minh, W-IQ-TREE: a fast online phylogenetic tool for maximum likelihood analysis. *Nucleic Acids Res.* **44**, W232-W235 (2016).
52. I. Letunic, P. Bork, Interactive Tree Of Life (iTOL) v5: an online tool for phylogenetic tree display and annotation. *Nucleic Acids Res.* **49**, W293-W296 (2021).
53. R. Zheng, R. Cai, C. Wang, R. Liu, C. Sun, Characterization of the first cultured representative of "*Candidatus* Thermofonsia" Clade 2 within *Chloroflexi* reveals its phototrophic lifestyle. *mBio* **13**, e0028722 (2022).
54. A. M. Bolger, M. Lohse, B. Usadel, Trimmomatic: a flexible trimmer for Illumina sequence data. *Bioinformatics* **30**, 2114-2120 (2014).
55. E. Kopylova, L. Noé, H. Touzet, SortMeRNA: fast and accurate filtering of ribosomal RNAs in metatranscriptomic data. *Bioinformatics* **28**, 3211-3217 (2012).
56. H. Li, R. Durbin, Fast and accurate short read alignment with Burrows-Wheeler transform. *Bioinformatics* **25**, 1754-1760 (2009).
57. A. R. Quinlan, BEDTools: The Swiss-Army Tool for Genome Feature Analysis. *Curr. Protoc. Bioinf.* **47**, 11.12.11-34 (2014).
58. J. Boulegue, Solubility of Elemental Sulfur in Water at 298-K. *Phosphorus, Sulfur Silicon Relat. Elem.* **5**, 127-128 (1978).
59. C. Gagnon, A. Mucci, E. Pelletier, Vertical distribution of dissolved sulphur species in coastal marine sediments. *Mar. Chem.* **52**, 195-209 (1996).
60. R. Cai, W. He, J. Zhang, R. Liu, Z. Yin, X. Zhang, C. Sun, Blue light promotes zero-valent sulfur production in a deep-sea bacterium. *EMBO J* **42**, e112514 (2023).

61. M. G. Murray, W. F. Thompson, Rapid isolation of high molecular-weight plant DNA. *Nucleic Acids Res.* **8**, 4321-4325 (1980).
62. T. Magoc, S. L. Salzberg, FLASH: fast length adjustment of short reads to improve genome assemblies. *Bioinformatics* **27**, 2957-2963 (2011).
63. N. A. Bokulich, S. Subramanian, J. J. Faith, D. Gevers, J. I. Gordon, R. Knight, D. A. Mills, J. G. Caporaso, Quality-filtering vastly improves diversity estimates from Illumina amplicon sequencing. *Nat. Methods* **10**, 57-59 (2013).
64. R. C. Edgar, B. J. Haas, J. C. Clemente, C. Quince, R. Knight, UCHIME improves sensitivity and speed of chimera detection. *Bioinformatics* **27**, 2194-2200 (2011).
65. R. C. Edgar, UPARSE: highly accurate OTU sequences from microbial amplicon reads. *Nat. Methods* **10**, 996-998 (2013).
66. C. Quast, E. Pruesse, P. Yilmaz, J. Gerken, T. Schweer, P. Yarza, J. Peplies, F. O. Glockner, The SILVA ribosomal RNA gene database project: improved data processing and web-based tools. *Nucleic Acids Res.* **41**, D590-D596 (2013).